SUPPLEMENTARY INFORMATION

The new ^{14}C chronology for the Palaeolithic site of La Ferrassie, France. The disappearance of Neandertals and the arrival of *Homo sapiens* in France.

Sahra Talamo, Vera Aldeias, Paul Goldberg, Laurent Chiotti, Harold L. Dibble, Guillaume Guérin, Jean-Jacques Hublin, Stephane Madelaine, Raquel Maria, Dennis Sandgathe, Teresa E. Steele, Alain Turq and Shannon J.P. McPherron

Content

Explanation of the Layer 4/5 radiocarbon age inversion, geological point of view

Vera Aldeias and Paul Goldberg

Geological evidence supporting the inversion: Some support for this hypothesis comes from the fact that Layer 5 is derived from an elevated source that is located in the direction of the apex of a colluvial cone to the NW; this source is no longer present, having been destroyed by road construction, and possibly by excavation and quarrying. In addition, Layer 4 is somewhat more decalcified than Layer 5, and thus this decalcification could represent incipient pedogenesis resulting from surface exposure of these deposits and a lack of sedimentation at this interval.

Geological evidence not supporting the inversion:

1) The ages are tightly clustered, and it is difficult to visualise that erosion from a "point source" and contributing deposits to the fan, would provide such a tight cluster of dates and not have greater variability in ages, because sediments (and datable materials) could have come from anywhere upslope. In other words, from a geological standpoint, it is difficult to rework "Layer 5" sediments from above as one unified body with tightly clustered dates. Moreover, the contacts between Layers 4 and 5 are conformable, and no significant erosional contacts between these layers were observed, although locally, the contact between Layers 3 and 4 is sharp.
2) Another possibility is that the dates for Layer 4 are too young for some reason. They might be misattributed, possibly because of a taphonomic issue. For example, a bone from the back dirt of Peyrony and Capitan's original excavations could have been trampled into Layer 4, in the areas where back dirt from previous excavations are closed to or directly above Layer 4 (particularly to the south of grid line I). Near the northern profile, the proximity to the cave's wall could represent the mixing of material, the so-called 'wall effect'. Both are rather common taphonomic issues in cave sites such as La Ferrassie.

FTIR

Raquel Maria

Figure S1 – FTIR spectra of extracted collagen samples from different layers. All samples show the three major characteristic collagen peaks at a) 1655 cm^{-1} (amide I), b) 1548 cm^{-1} (amide II) and 1452 cm^{-1} (amino acid proline absorption). No additional peaks are observed.

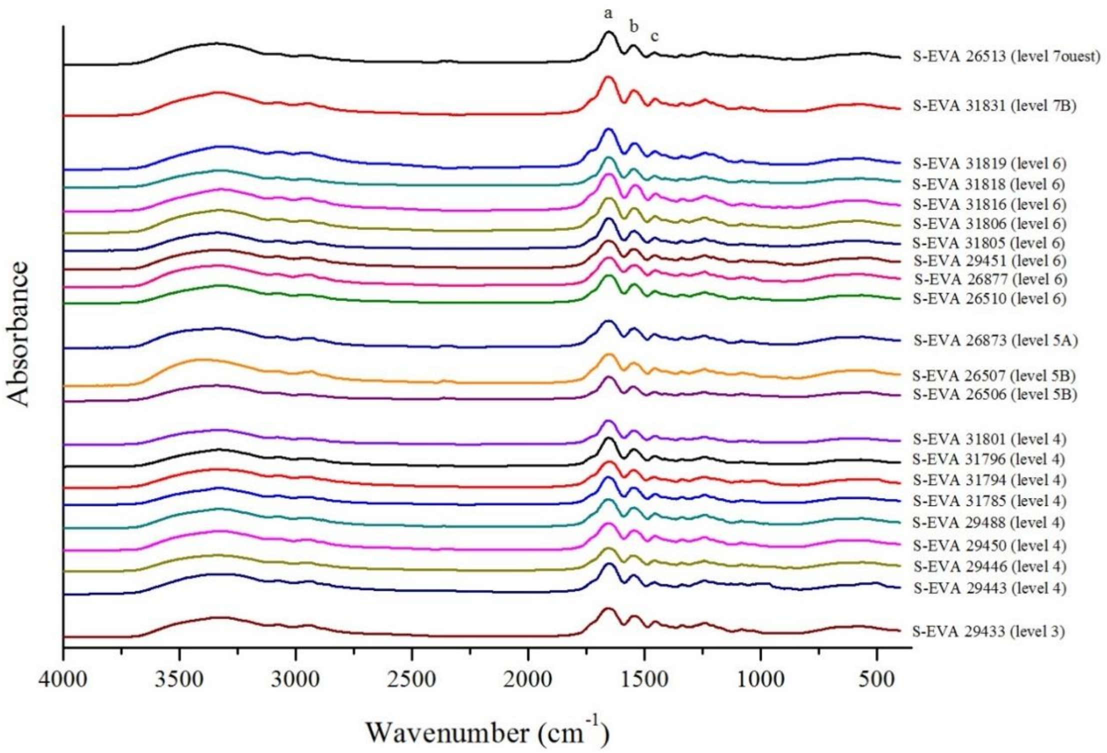

Sites descriptions, Tables of the duration of the phases, and the CQL codes

Sahra Talamo

La Ferrassie
See the main text for the site description

Table S2: Bayesian Modelled calibrated ages and Boundaries of Model 1 provided by the IntCal13 using OxCal 4.3 program (Reimer et al., 2013, Ramsey, 2009). In red are the six samples, which are excluded from the model iterations by giving them a prior outlier probability of 100%.

Indices Amodel 3.8 Aoverall 4.8	**Un-Modelled (BP)**				**Modelled (BP)**				**Outliers Posterior**
La Ferrassie Sequence	**Cal BP 68.2%**		**Cal BP 95.4%**		**Cal BP 68.2%**		**Cal BP 95.4%**		
	from	**to**	**from**	**to**	**from**	**to**	**from**	**to**	
End Layer 9 Boundary					29340	28020	29510	26080	
MAMS-25530 (25120,120)	29340	28980	29500	28830	29370	28990	29580	28780	
MAMS-25529 (27070,150)	31200	30980	31300	30860	31110	28770	31200	27890	88%
Layer 9 Under Study Phase									
Transition Layer 8/9 Boundary					30630	29340	31230	29070	
MAMS-25528(27160,150)	31240	31020	31350	30910	31240	31000	31410	30810	
MAMS-25527 (26270,130)	30780	30450	30910	30250	30840	30440	31570	30150	
Layer 8 Under Study Phase									
Start Layer 8 Boundary					32590	30990	35450	30870	
End Layer 7 Boundary					36850	36140	37240	35600	
MAMS-25525 (32810,270)	37220	36350	37860	36160	37180	36540	37610	36310	
MAMS-25526 (33730,290)	38590	37790	38830	37120	37600	36750	38300	36550	
MAMS-16377 (32980,240)	37490	36580	38010	36350	37270	36630	37710	36410	
MAMS-16374 (32610,230)	36810	36220	37410	36000	37020	36420	37440	36220	
MAMS-25521 (32510,240)	36700	36120	37220	35820	37000	36380	37430	36150	

MAMS-25520 (33100,260)	37730	36740	38210	36460	37330	36660	37820	36450	
MAMS-16375 (32250,230)	36390	35890	36670	35600	37330	36530	37980	36070	100% Wall effect
MAMS-16376 (33090,240)	37690	36750	38160	36470	37320	36670	37790	36470	
MAMS-17584 (35206,160)	40020	39550	40240	39310	37430	36550	38270	36180	100% Wall effect
Layer 7 Aurignacian Phase									
Start Layer 7 Boundary					37940	36890	38730	36690	
End Layer 6 Boundary					41390	39270	41640	37680	
MAMS-21206 (40890,500)	44920	43950	45350	43460	44810	43950	45060	43430	
MAMS-25524 (40770,650)	44910	43700	45500	43190	44760	43710	45050	43190	
MAMS-21208 (36300,300)	41300	40620	41570	40270	43240	40420	44820	39520	100% Wall effect
MAMS-25523 (39000,510)	43240	42490	43790	42170	43260	42470	43910	42130	
MAMS-25522 (36590,390)	41610	40850	41900	40410	41700	40920	42050	40380	
MAMS-21207 (38910,390)	43080	42520	43420	42250	44290	41380	45030	40240	100% Wall effect
MAMS-17585 (32450,130)	36480	36170	36700	36010	42810	39600	44380	38390	100% Wall effect
MAMS-16373 (37380,390)	42130	41550	42420	41240	42140	41540	42490	41170	
Layer 6 Châtelperronian Phase									
Transition Layer 5/6 Boundary					45170	44790	45370	44540	
MAMS-17583 (42010,310)	45660	45050	45970	44770	45230	44890	45430	44710	
MAMS-21209 (39740,430)	43810	43010	44280	42750	45230	44870	45430	44660	100% Wall effect
MAMS-16381 (43370,300)	46880	46130	47330	45820	45230	44870	45450	44660	97%
MAMS-16371 (42150,660)	46080	44890	46870	44360	45230	44880	45430	44690	
MAMS-16372 (42370,680)	46300	45050	47180	44510	45230	44880	45440	44690	
MAMS-17581 (42360,330)	45950	45310	46310	45010	45240	44890	45450	44710	
MAMS-17582 (43520,380)	47130	46200	47700	45860	45230	44870	45450	44670	97%
MAMS-17580 (41680,310)	45400	44790	45700	44500	45220	44880	45420	44700	
Layer 5 Middle Palaeolithic/Mousterian Phase									
Transition Layer 4/5 Boundary					45300	44940	45520	44760	
MAMS-25519 (39180,520)	43390	42590	43990	42290	45390	44990	45680	44800	94%

MAMS-25516 (40800,620)	44920	43750	45470	43250	45380	44990	45630	44810	
MAMS-21205 (38050,360)	42520	42020	42780	41770	45390	44990	45680	44800	100% Wall effect
MAMS-25518 (40220,590)	44360	43290	44950	42900	45370	44990	45640	44800	18%
MAMS-21203 (41400,520)	45340	44410	45840	43920	45380	44990	45640	44810	
MAMS-21198 (39980,440)	44030	43200	44480	42900	45380	44980	45680	44800	72%
MAMS-21204 (40970,500)	44990	44030	45430	43530	45370	44990	45630	44810	
Layer 4 Middle Palaeolithic/Mousterian Phase									
Transition Layer 3/4 Boundary					45490	45020	45860	44830	
MAMS-21196 (43140,640)	47020	45690	47950	45220	47040	45730	48000	45330	
MAMS-21195 (47480,1060)	...	49670	...	49950	50010	49000	50010	47660	
MAMS-21194 (45280,820)	49600	47890	...	47130	49420	47660	50010	46940	
Layer 3 Middle Palaeolithic/Mousterian Phase									
Transition Layer 2/3 Boundary					51240	48980	54190	47820	
Layer 2 Middle Palaeolithic/Mousterian Phase									
Transition Layer 1/2 Boundary					55220	49580	62890	48300	
Layer 1 Middle Palaeolithic/Mousterian Phase									
Start Layer 1 Boundary					58990	50580	69790	49130	

Table S3: Bayesian Modelled calibrated ages and Boundaries of Model 2 provided by the IntCal13 (Reimer et al., 2013) using OxCal 4.3 (Ramsey, 2009). In red are the six samples, which are excluded from the model iterations by giving them a prior outlier probability of 100%. For a figure of the sequences, see Fig. 2 in the main text.

Indices Amodel 43,9 Aoverall 51,5	**Un-Modelled (BP)**				**Modelled (BP)**				**Outliers Posterior**
La Ferrassie Sequence	**Cal BP 68.2%**		**Cal BP 95.4%**		**Cal BP 68.2%**		**Cal BP 95.4%**		
	from	**to**	**from**	**to**	**from**	**to**	**from**	**to**	
End Layer 9 Boundary					29360	28110	29510	26240	
MAMS-25530 (25120,120)	29340	28980	29500	28830	29380	29000	29570	28820	
MAMS-25529 (27070,150)	31200	30980	31300	30860	31050	28830	31180	28030	90%
Layer 9 Under Study Phase									
Transition Layer 8/9 Boundary					30630	29370	31190	29110	
MAMS-25528(27160,150)	31240	31020	31350	30910	31240	31010	31360	30870	
MAMS-25527 (26270,130)	30780	30450	30910	30250	30840	30450	31350	30210	
Layer 8 Under Study Phase									
Start Layer 8 Boundary					32520	30980	35280	30870	
End Layer 7 Boundary					36860	36150	37250	35610	
MAMS-25525 (32810,270)	37220	36350	37860	36160	37180	36540	37620	36310	
MAMS-25526 (33730,290)	38590	37790	38830	37120	37620	36750	38310	36560	
MAMS-16377 (32980,240)	37490	36580	38010	36350	37260	36630	37700	36410	
MAMS-16374 (32610,230)	36810	36220	37410	36000	37030	36420	37440	36210	
MAMS-25521 (32510,240)	36700	36120	37220	35820	37000	36370	37420	36150	
MAMS-25520 (33100,260)	37730	36740	38210	36460	37330	36660	37830	36460	
MAMS-16375 (32250,230)	36390	35890	36670	35600	37340	36530	38030	36070	100% Wall effect
MAMS-16376 (33090,240)	37690	36750	38160	36470	37320	36670	37800	36470	
MAMS-17584 (35206,160)	40020	39550	40240	39310	37450	36560	38320	36170	100% Wall effect
Layer 7 Aurignacian Phase									
Start Layer 7 Boundary					37950	36860	38790	36680	
End Layer 6 Boundary					41500	39450	41740	37730	

MAMS-21206 (40890,500)	44920	43950	45350	43460	44730	43860	45080	43370	
MAMS-25524 (40770,650)	44910	43700	45500	43190	44670	43630	45090	43130	
MAMS-21208 (36300,300)	41300	40620	41570	40270	43360	40510	44830	39590	100% Wall effect
MAMS-25523 (39000,510)	43240	42490	43790	42170	43250	42480	43900	42140	
MAMS-25522 (36590,390)	41610	40850	41900	40410	41710	40960	42060	40420	
MAMS-21207 (38910,390)	43080	42520	43420	42250	44380	41390	45060	40180	100% Wall effect
MAMS-17585 (32450,130)	36480	36170	36700	36010	43230	39880	44560	38440	100% Wall effect
MAMS-16373 (37380,390)	42130	41550	42420	41240	42140	41550	42480	41190	
Layer 6 Châtelperronian Phase									
Transition Layer 5/6 Boundary					45300	44620	45590	44170	
MAMS-17583 (42010,310)	45660	45050	45970	44770	45710	45150	46010	44890	
MAMS-21209 (39740,430)	43810	43010	44280	42750	46150	45040	46740	44550	100% Wall effect
MAMS-16381 (43370,300)	46880	46130	47330	45820	46530	45910	46920	45570	
MAMS-16371 (42150,660)	46080	44890	46870	44360	46010	45160	46500	44800	
MAMS-16372 (42370,680)	46300	45050	47180	44510	46110	45240	46590	44870	
MAMS-17581 (42360,330)	45950	45310	46310	45010	45940	45340	46260	45080	
MAMS-17582 (43520,380)	47130	46200	47700	45860	46580	45890	47010	45510	
MAMS-17580 (41680,310)	45400	44790	45700	44500	45560	45000	45860	44710	
Layer 5 Middle Palaeolithic/Mousterian Phase									
Transition Layer 4/5 Boundary					46910	46130	47470	45780	
Layer 4 Middle Palaeolithic/Mousterian Phase									
Transition Layer 3/4 Boundary					48060	46530	49140	46160	
MAMS-21196 (43140,640)	47020	45690	47950	45220	48590	46970	49650	46500	17%
MAMS-21195 (47480,1060)	...	49670	...	49950	50010	48720	50010	47670	
MAMS-21194 (45280,820)	49600	47890	...	47130	49370	47870	49960	47310	
Layer 3 Middle Palaeolithic/Mousterian Phase									
Transition Layer 2/3 Boundary					50580	48540	52390	47460	

Layer 2 Middle Palaeolithic/Mousterian Phase									
Transition Layer 1/2 Boundary					53990	48970	60680	47680	
Layer 1 Middle Palaeolithic/Mousterian Phase									
Start Layer 1 Boundary					58070	49710	66880	48120	

Bayesian Modelled Boundaries and Duration of the phases provided by the IntCal13 (Reimer et al., 2013) using OxCal 4.3 program (Ramsey, 2009) are the following:

La Ferrassie Model 1 (including dates on layer 4)	**Modelled (BP)**			
	Cal BP 68.2%		**Cal BP 95.4%**	
	from	**to**	**from**	**to**
End Layer 7	36850	36140	37240	35600
Layer 7 Aurignacian	37370	36540	38120	36080
Start Layer 7	37940	36890	38730	36690
End Layer 6	41390	39270	41640	37680
Layer 6 Châtelperronian	44670	41350	45100	39520
Transition Layer 5/6	45170	44790	45370	44540
Transition Layer 5/6	45170	44790	45370	44540
Layer Middle Palaeolithic/Mousterian	52400	45050	60870	44720
Start Layer 1	58990	50580	69790	49130

La Ferrassie Model 2 (not including dates on layer 4)	**Modelled (BP)**			
	Cal BP 68.2%		**Cal BP 95.4%**	
	from	**to**	**from**	**to**
End Layer 7	36860	36150	37250	35610
Layer 7 Aurignacian	37370	36530	38150	36080
Start Layer 7	37950	36860	38790	36680
End Layer 6	41500	39450	41740	37730
Layer 6 Châtelperronian	44490	41250	45180	39520
Transition Layer 5/6	45300	44620	45590	44170
Transition Layer 5/6	45300	44620	45590	44170
Layer Middle Palaeolithic/Mousterian	51820	45060	59360	44450
Start Layer 1	58070	49710	66880	48120

In red are the ranges taken for building the bars in the graph in Figure 3 in the main text

CQL Code:

```
Plot()
 {
  Outlier_Model("General",T(5),U(0,4),"t");
  Sequence("La Ferrassie Model 2")
  {
   Boundary("Start Layer 1");
   Phase("Layer 1 Mousterian")
   {
```

```
};
Boundary("Transition Layer 1/2");
Phase("Layer 2 Mousterian")
{
};
Boundary("Transition Layer 2/3");
Phase("Layer 3 Mousterian")
{
 R_Date("MAMS-21194", 45280, 820)
 {
  Outlier(0.05);
 };
 R_Date("MAMS-21195", 47480, 1060)
 {
  Outlier(0.05);
 };
 R_Date("MAMS-21196", 43140, 640)
 {
  Outlier(0.05);
 };
};
Boundary("Transition Layer 3/4");
Phase("Layer 4")
{
};
Boundary("Transition Layer 4/5");
Phase("Layer 5")
{
 R_Date("MAMS-17580", 41680, 310)
 {
  Outlier(0.05);
 };
 R_Date("MAMS-17582", 43520, 380)
 {
  Outlier(0.05);
 };
 R_Date("MAMS-17581", 42360, 330)
 {
  Outlier(0.05);
 };
 R_Date("MAMS-16372", 42370, 680)
 {
  Outlier(0.05);
 };
 R_Date("MAMS-16371", 42150, 660)
 {
  Outlier(0.05);
 };
 R_Date("MAMS-16381", 43370, 300)
 {
  Outlier(0.05);
```

```
 };
 R_Date("MAMS-21209", 39740, 430)
 {
  Outlier(1.0);
 };
 R_Date("MAMS-17583", 42010, 310)
 {
  Outlier(0.05);
 };
};
Boundary("Transition Layer 5/6");
Phase("Layer 6 Chatelperronian")
{
 R_Date("MAMS-16373", 37380, 390)
 {
  Outlier(0.05);
 };
 R_Date("MAMS-17585", 32450, 130)
 {
  Outlier(1.0);
 };
 R_Date("MAMS-21207", 38910, 390)
 {
  Outlier(1.0);
 };
 R_Date("MAMS-25522", 36590, 390)
 {
  Outlier(0.05);
 };
 R_Date("MAMS-25523", 39000, 510)
 {
  Outlier(0.05);
 };
 R_Date("MAMS-21208", 36300, 300)
 {
  Outlier(1.0);
 };
 R_Date("MAMS-25524", 40770, 650)
 {
  Outlier(0.05);
 };
 R_Date("MAMS-21206", 40890, 500)
 {
  Outlier(0.05);
 };
};
Boundary("End Layer 6");
Boundary("Start Layer 7");
Phase("Layer 7 Aurignacian")
{
 R_Date("MAMS-17584", 35206, 160)
```

```
 {
  Outlier(1.0);
 };
 R_Date("MAMS-16376", 33090, 240)
 {
  Outlier(0.05);
 };
 R_Date("MAMS-16375", 32250, 230)
 {
  Outlier(1.0);
 };
 R_Date("MAMS-25520", 33100, 260)
 {
  Outlier(0.05);
 };
 R_Date("MAMS-25521", 32510, 240)
 {
  Outlier(0.05);
 };
 R_Date("MAMS-16374", 32610, 230)
 {
  Outlier(0.05);
 };
 R_Date("MAMS-16377", 32980, 240)
 {
  Outlier(0.05);
 };
 R_Date("MAMS-25526", 33730, 290)
 {
  Outlier(0.05);
 };
 R_Date("MAMS-25525", 32810, 270)
 {
  Outlier(0.05);
 };
};
Boundary("End Layer 7");
Boundary("Start Layer 8");
Phase("Layer 8 Under Study")
{
 R_Date("MAMS-25527", 26270, 130)
 {
  Outlier(0.05);
 };
 R_Date("MAMS-25528", 27160, 150)
 {
  Outlier(0.05);
 };
};
Boundary("Transitional Layer 8/9");
Phase("Layer 9 Under Study")
```

```
  {
   R_Date("MAMS-25529", 27070, 150)
   {
    Outlier(0.05);
   };
   R_Date("MAMS-25530", 25120, 120)
   {
    Outlier(0.05);
   };
  };
  Boundary("End Layer 9");
 };
 Sequence()
 {
  Boundary("=Start Layer 1");
  Date("Layer Mousterian");
  Boundary("=Transition Layer 5/6");
 };
 Sequence()
 {
  Boundary("=Transition Layer 5/6");
  Date("Layer 6 Chatelperronian");
  Boundary("=End Layer 6");
 };
 Sequence()
 {
  Boundary("=Start Layer 7");
  Date("Layer 7 Aurignacian");
  Boundary("=End Layer 7");
 };
};
```

Poitou-Charentes region

La Quina Amont and Aval:

La Quina (Charente) is divided into two areas, Aval and Amont. The Amont area has yielded archaeological evidence attributed only to Middle Palaeolithic (Mousterian). The Bayesian model is taken from Frouin et al. (2017).

Bayesian Modelled Boundaries and Duration of the phases provided by the IntCal13 (Reimer et al., 2013) using OxCal 4.3 (Ramsey, 2009) are the following:

La Quina Amont Sequence	**Modelled (BP)**			
Indices Amodel 44.3 Aoverall 51.2	**from**	**to**	**from**	**to**
	68,20%		**95,40%**	
End phase 1	41460	38950	42120	36360
Mousterian	47800	41340	49890	39200
Start level 8	50290	48160	51320	47080

In red are the ranges taken for building the bars in the graph in Figure 3 in the main text

CQL Code:

```
Plot()
 {
  Outlier_Model("General",T(5),U(0,4),"t");
  Sequence("La Quina Amont sequence")
  {
   Boundary("Start level 8");
   Phase("Level 8")
   {
    R_Date("OxA-21807", 45200, 2200)
    {
     Outlier(0.05);
    };
    Age("Q14", N( 44500, 4200))
    {
     Outlier(0.05);
    };
    Age("Q15", N( 53000, 5000))
    {
     Outlier(0.05);
    };
    Age("BDX-15262", N( 51000, 3880))
    {
     Outlier(0.05);
    };
   };
   Boundary("8/7");
   Phase("Level 7")
   {
    R_Date("OxA-22155", 48900, 3400)
    {
     Outlier(0.05);
    };
    Age("BDX-15261", N( 50200, 2860))
    {
     Outlier(0.05);
    };
   };
   Boundary("7/6d");
   Phase("Level 6d")
   {
    R_Date("OxA-21808", 44200, 1900)
    {
     Outlier(0.05);
    };
   };
   Boundary("6d/6c");
   Boundary("6b/6a");
   Phase("Level 6a")
   {
    R_Date("OxA-21806", 36850, 800)
```

```
   {
    Outlier(0.05);
   };
   Age("Q1-Q3", N( 43000, 3600))
   {
    Outlier(0.05);
   };
   Age("BDX-15259", N( 44900, 2550))
   {
    Outlier(0.05);
   };
  };
  Boundary("6a/5");
  Phase("Level 5")
  {
   R_Date("OxA-21805", 41100, 1300)
   {
    Outlier(0.05);
   };
  };
  Boundary("Transition 5/4b");
  Phase("Level 4b")
  {
   R_Date("OxA-22153", 37500, 800)
   {
    Outlier(0.05);
   };
  };
  Boundary("4b/3");
  Boundary("3/2a");
  Phase("Level 2b")
  {
   R_Date("OxA-X-2326-22", 37000, 800)
   {
    Outlier(0.05);
   };
  };
  Boundary("2a/1");
  Boundary("End phase 1");
 };
 Sequence()
 {
  Boundary("=Start level 8");
  Date("Mousterian");
  Boundary("=End phase 1");
 };
};
```

The Aval area has yielded archaeological evidence attributed to Châtelperronian and Aurignacian. Since these are two separate areas (Amont and Aval), and because the Châtelperronian does not occur in Amont, we modelled the two dates of the Châtelperronian provided by Higham et al.

(2014) together with the only date provided in Verna et al. (2012) for the Aurignacian on top. This Bayesian model does not provide a realistic output for the Aurignacian, which is based on only one date.

Bayesian Modelled Boundaries and Duration of the phases provided by the IntCal13 (Reimer et al., 2013) using OxCal 4.3 (Ramsey, 2009) are the following:

La Quina Aval sequence	**Modelled (BP)**			
Indices Amodel 103.3 Aoverall 104.9	**from**	**to**	**from**	**to**
	68,20%		**95,40%**	
End Châtelperronian	42950	41170	43610	39130
Châtelperronian	43470	41800	45100	40250
Start Châtelperronian	44090	42310	46580	41820
End Aurignacian	38200	36240	38600	32700
Aurignacian	38660	36760	40720	34840
Start Aurignacian	39420	37230	41520	36800

In red are the ranges taken for building the bars in the graph in Figure 3 in the main text

CQL Code:

```
Plot()
 {
  Outlier_Model("General",T(5),U(0,4),"t");
  Sequence("La Quina Aval sequence")
  {
   Boundary("Start Chatelperronian");
   Phase("Chatelperronian")
   {
    R_F14C("OxA-21706",0.00741,0.00096)
    {
     Outlier(0.05);
    };
    R_F14C("OxA-21707",0.00873,0.00099)
    {
     Outlier(0.05);
    };
   };
   Boundary("End Chatelperronian");
   Boundary("Start Aurignacian");
   Phase("Aurignacian")
   {
    R_Date("OxA15054 ", 33290, 330);
   };
   Boundary("End Aurignacian");
  };
  Sequence()
  {
   Boundary("=Start Aurignacian");
```

```
 Date("Aurignacian");
 Boundary("=End Aurignacian");
};
Sequence()
{
 Boundary("=Start Chatelperronian");
 Date("Chatelperronian");
 Boundary("=End Chatelperronian");
};
};
```

Saint Césaire
Saint Césaire is located in the Charente region of France. Neandertal remains were discovered in layer EJOP. This layer is divided into *inf* and *sup*, respectively Mousterian and Châtelperronian. This attribution was recently challenged by Gravina et al. (2018), where they confirmed that the EJOP*inf* is of Mousterian attribution, but the EJOP*sup* is a mix between Mousterian and Châtelperronian industries. They conclude that the attribution to the Neandertal remains to one or the other is questionable. This site contains an upper level of Protoaurignacian.

Bayesian Modelled Boundaries and Duration of the phases provided by the IntCal13 (Reimer et al., 2013) using OxCal 4.3 (Ramsey, 2009) are the following:

Saint Césaire Boundaries	**Modelled (BP)**			
Indices Amodel 29.6 Aoverall 32.4	**from**	**to**	**from**	**to**
	68,20%		**95,40%**	
EJO sup/EJF	38150	36810	38450	35560
Protoaurignacian	38480	37300	39160	36390
EJO inf/EJO sup	38970	37740	39840	37140
EJOP sup/EJO inf	41150	39840	41540	38770
Châtelperronian	41600	40430	42280	39570
EJOPinf/EJOP sup	42140	40970	42910	40480
Transition EGPF/EJOPinf	43770	42250	44760	41600
Mousterian	45340	42790	47720	41970
Start EGF	47110	43580	50020	42460

In red are the ranges taken for building the bars in the graph in Figure 3 in the main text

CQL Code:

```
Options()
{
 Resolution=20;
 Plot()
 {
  Outlier_Model("General",T(5),U(0,4),"t");
  Sequence()
  {
   Boundary("Start EGF");
```

```
Phase("EGF Denticulate Mousterian")
{
 Age("", N( 42400, 4800))
 {
  Outlier(0.05);
 };
};
Boundary("EGF/EGP");
Phase("EGP Denticulate Mousterian")
{
 Age("", N( 38200, 3300))
 {
  Outlier(0.05);
 };
};
Boundary("End EGP/Start EGPF");
Phase("EGPF Denticulate Mousterian")
{
 R_F14C("OxA-21638",0.00507,0.00134)
 {
  Outlier(0.05);
 };
 Age("", N( 40900, 2500))
 {
  Outlier(0.05);
 };
};
Boundary("Transition EGPF/EJOPinf");
Phase("EJOPinf Chatelperronian?")
{
 R_F14C("OxA-21637",0.00681,0.0016)
 {
  Outlier(0.05);
 };
};
Boundary("EJOPinf/EJOP sup");
Phase("Chatelperronian EJOP sup")
{
 Age("", N( 36300, 2700))
 {
  Outlier(0.05);
 };
 R_F14C("OxA-21636",0.00978,0.00125)
 {
  Outlier(0.05);
 };
 R_F14C("OxA-21699",0.01132,0.00098)
 {
  Outlier(0.05);
 };
 R_F14C("OxA-21700",0.01043,0.00097)
```

```
  {
   Outlier(0.05);
  };
  R_F14C("OxA-18099",0.01102,0.00102)
  {
   Outlier(0.05);
  };
 };
 Boundary("EJOP sup/EJO inf");
 Phase("Aurignacian? EJO inf")
 {
 };
 Boundary("EJO inf/EJO sup");
 Phase("Protoaprourignacian EJO sup")
 {
  R_F14C("OxA-21633",0.01805,0.00133)
  {
   Outlier(0.05);
  };
  R_F14C("OxA-21628", 0.01572, 0.00101)
  {
   Outlier(0.05);
  };
  R_F14C("OxA-21634", 0.01381, 0.00131)
  {
   Outlier(0.05);
  };
  R_F14C("OxA-21635", 0.01584, 0.00134)
  {
   Outlier(0.05);
  };
  R_F14C("OxA-21629", 0.01448, 0.00101)
  {
   Outlier(0.05);
  };
  Age("", N( 32100, 3000))
  {
   Outlier(0.05);
  };
 };
 Boundary("EJO sup/EJF");
};
Sequence()
{
 Boundary("=Start EGF");
 Date("Mousterian");
 Boundary("=Transition EGPF/EJOPinf");
};
Sequence()
{
 Boundary("=EJOPinf/EJOP sup");
```

```
  Date("Chatelperronian");
  Boundary("=EJOP sup/EJO inf");
 };
 Sequence()
 {
  Boundary("=EJO inf/EJO sup");
  Date("Protoaurignacian");
  Boundary("=EJO sup/EJF");
 };
};
};
```

Aquitaine region

Le Moustier

Le Mousterier is a Middle-Upper Palaeolithic site in the Dordogne region, close to Vézère River, in southwestern France. The site has yielded archaeological evidence attributed to Mousterian, Châtelperronian and Aurignacian. From the bottom to the top there is: Layer G (MTA-A), Layer H (MTA-B, **not** Châtelperronian affiliation (Gravina and Discamps, 2015)), Layer I (Denticulate Mousterian), Layer J (Typical Mousterian), Layer K (Châtelperronian-lower Aurignacian) and the top Layer L with Middle Aurignacian. The model was built following Higham et al. (2014). However, the range of the Châtelperronian is based only on one TL date in Layer K. This could display an artefact boundary due to the wide error range.

Bayesian Modelled Boundaries and Duration of the phases provided by the IntCal13 (Reimer et al., 2013) using OxCal 4.3 (Ramsey, 2009) are the following:

Le Moustier Boundaries	**Modelled (BP)**			
Indices Amodel 33.1 Aoverall 34.8	**from**	**to**	**from**	**to**
	68,20%		**95,40%**	
End Châtelperronian	44100	40160	45270	37310
Châtelperronian	44080	41080	45310	39100
Transition J/K	44220	41820	45280	40770
Transition J/K	44220	41820	45280	40770
Mousterian	47600	43810	49480	42010
Start Level G	49690	46730	51320	46010

In red are the ranges taken for building the bars in the graph in Figure 3 in the main text

CQL Code:

```
Plot()
 {
  Outlier_Model("General",T(5),U(0,4),"t");
  Sequence()
  {
   Boundary("Start Level G");
   Phase("G MTA A")
   {
```

```
 Age("", N( 50300, 5500))
 {
  Outlier(0.05);
 };
 R_F14C("OxA-21790",0.00454,0.001)
 {
  Outlier(0.05);
 };
};
Boundary("Transition G/H");
Phase("H MTA B")
{
 R_F14C("OxA-21751",0.00412,0.00095)
 {
  Outlier(0.05);
 };
 R_F14C("OxA-21752",0.00359,0.00097)
 {
  Outlier(0.05);
 };
 Age("", N( 42500, 2000))
 {
  Outlier(0.05);
 };
 Age("", N( 46300, 3000))
 {
  Outlier(0.05);
 };
 R_F14C("OxA-21750",0.00198,0.00097)
 {
  Outlier(0.05);
 };
 R_F14C("OxA-21791",0.0037,0.00098)
 {
  Outlier(0.05);
 };
};
Boundary("Transition H/I");
Phase("I")
{
 R_F14C("OxA-21753",0.00457,0.00097)
 {
  Outlier(0.05);
 };
 Age("", N( 40900, 5000))
 {
  Outlier(0.05);
 };
};
Boundary("Transition I/J");
Phase("J Typical Mousterian")
```

```
  {
   R_F14C("OxA-X-2300-19",0.00927,0.00102)
   {
    Outlier(0.05);
   };
   R_F14C("OxA-21754",0.00366,0.00104)
   {
    Outlier(0.05);
   };
   R_F14C("OxA-X-2300-21",0.00632,0.001)
   {
    Outlier(0.05);
   };
   R_F14C("OxA-21765",0.00635,0.00142)
   {
    Outlier(0.05);
   };
   Age("", N( 40300, 2600))
   {
    Outlier(0.05);
   };
   R_F14C("OxA-21789",0.00654,0.00097)
   {
    Outlier(0.05);
   };
  };
  Boundary("Transition J/K");
  Phase("K Chatelperronian")
  {
   Age("", N( 42600, 3200))
   {
    Outlier(0.05);
   };
  };
  Boundary("End CP");
 };
 Sequence()
 {
  Boundary("=Start Level G");
  Date("Mousterian");
  Boundary("=Transition J/K");
 };
 Sequence()
 {
  Boundary("=Transition J/K");
  Date("Chatelperronian");
  Boundary("=End CP");
 };
};
```

Pech de l'Aze IV

Pech IV is a Middle Palaeolithic site located in the Dordogne region of southwest France. There is no evidence of Châtelperronian, Protoaurignacian or Aurignacian. The model built is still the one published in McPherron et al. (2012), adding the previously not included ^{14}C Age of 47,400±650 (OxA-V-2344-16).

Bayesian Modelled Boundaries and Duration of the phase provided by the IntCal13 (Reimer et al., 2013) using OxCal 4.3 (Ramsey, 2009) are the following:

Pech IV	**Modelled (BP)**			
Indices Amodel 86.9 Aoverall 83.5	**from**	**to**	**from**	**to**
	68,20%		**95,40%**	
End A	46570	40900	46630	39510
Mousterian	49160	44410	50790	41530
Start B	51320	46480	52520	46420

In red are the ranges taken for building the bars in the graph in Figure 3 in the main text

CQL Code:

```
Plot()
 {
  Outlier_Model("General",T(5),U(0,4),"t");
  Sequence(Pech IV)
  {
   Boundary("Start B");
   Phase("A/B")
   {
    R_Date("OxA-V-2344-16", 47400, 650)
    {
     Outlier(0.05);
    };
    R_Date("OxA-V-2344-17", 40760, 400)
    {
     Outlier(0.05);
    };
    R_Date("OxA-V-2344-14", 42930, 450)
    {
     Outlier(0.05);
    };
    R_Date("OxA-V-2344-18", 42690, 500)
    {
     Outlier(0.05);
    };
    R_Date("OxA-V-2344-11", 43050, 400)
    {
     Outlier(0.05);
    };
    R_Date("OxA-V-2333-35", 44720, 700)
    {
     Outlier(0.05);
```

```
   };
   R_Date("OxA-V-2344-12", 43910, 450)
   {
    Outlier(0.05);
   };
   R_Date("OxA-V-2344-13", 43720, 450)
   {
    Outlier(0.05);
   };
   R_Date("OxA-V-2333-36", 37400, 370)
   {
    Outlier(1.0);
   };
  };
  Boundary("End A");
 };
 Sequence()
 {
  Boundary("=Start B");
  Date("Mousterian");
  Boundary("=End A");
 };
};
```

Abri Pataud
Is an Upper Palaeolithic site in the Dordogne region, close to the Vézère River in southwestern France. It contains several Aurignacian layers (Early and Evolved) and an upper layer with Early Gravettian. The Bayesian model is still the one published in Higham et al. (2011).

Bayesian Modelled Boundaries and Duration of the phases provided by IntCal13 (Reimer et al., 2013) using OxCal 4.3 (Ramsey, 2009) are the following:

Abri Pataud Boundaries	**Modelled (BP)**			
Indices Amodel 81 Aoverall 89.4	**from**	**to**	**from**	**to**
	68,20%		**95,40%**	
Eboulis 4/5	32380	30720	32580	30460
Gravettian	32550	31560	32900	30850
Start 5	32780	31860	33490	31620
Eboulis 5/6	35360	34670	35650	33970
Evolved Aurignacian	36460	35230	37010	34650
Start 8	36980	36340	37400	36130
Eboulis 8/9	37380	36650	37760	36380
Early Aurignacian	39400	37490	39980	36860
Start Eboulis de Base	40150	39410	40610	39110

In red are the ranges taken for building the bars in the graph in Figure 3 in the main text

CQL Code:

```
Plot()
 {
  Outlier_Model("General",T(5),U(0,4),"t");
  Sequence("Abri Pataud")
  {
   Boundary("Start Eboulis de Base");
   Phase("Niveau 14")
   {
    R_Date("OxA-21579", 35000, 600)
    {
     Outlier(0.05);
    };
    R_Date("OxA-21578", 35750, 700)
    {
     Outlier(0.05);
    };
    R_Date("OxA-21597", 35000, 650)
    {
     Outlier(0.05);
    };
    R_Date("OxA-21596", 34500, 600)
    {
     Outlier(0.05);
    };
   };
   Boundary("Eboulis 13/14");
   Boundary("Start 13");
   Phase("Niveau 13")
   {
    R_Date("OxA-15216", 35400, 750)
    {
     Outlier(0.05);
    };
    R_Date("OxA-21600", 34200, 550)
    {
     Outlier(0.05);
    };
    R_Date("OxA-21599", 34850, 600)
    {
     Outlier(0.05);
    };
    R_Date("OxA-21598", 34750, 600)
    {
     Outlier(0.05);
    };
   };
   Boundary("Eboulis 12/13");
   Boundary("Start 12");
```

```
Phase("Niveau 12")
{
 R_Date("OxA-21672", 34050, 550)
 {
  Outlier(0.05);
 };
 R_Date("OxA-21671", 34300, 600)
 {
  Outlier(0.05);
 };
 R_Date("OxA-21670", 33450, 500)
 {
  Outlier(0.05);
 };
};
Boundary("Eboulis 11/12");
Boundary("Start 11");
Phase("Niveau 11")
{
 R_Date("OxA-21581", 33550, 550)
 {
  Outlier(0.05);
 };
 R_Date("OxA-21580", 33550, 550)
 {
  Outlier(0.05);
 };
 R_Date("OxA-21602", 33500, 500)
 {
  Outlier(0.05);
 };
 R_Date("OxA-21601", 34150, 550)
 {
  Outlier(0.05);
 };
};
Boundary("Eboulis 10/11");
Boundary("Start 10");
Phase("Niveau 10")
{
 R_Date("OxA-21679", 33650, 500)
 {
  Outlier(0.05);
 };
};
Boundary("Eboulis 9/10");
Boundary("Start 9");
Phase("Niveau 9")
{
 R_Date("OxA-21673", 33400, 500)
 {
```

```
  Outlier(0.05);
 };
};
Boundary("Eboulis 8/9");
Boundary("Start 8");
Phase("Niveau 8")
{
 R_Date("OxA-2276-19", 33050, 500)
 {
  Outlier(0.05);
 };
 R_Date("OxA-21582", 31300, 400)
 {
  Outlier(0.05);
 };
};
Boundary("Eboulis 7/8");
Boundary("Start 7");
Phase("Niveau 7")
{
 R_Date("GrN-3117", 32800, 450)
 {
  Outlier(0.05);
 };
 R_Date("OxA-X-2276-20", 32150, 450)
 {
  Outlier(0.05);
 };
 R_Date("OxA-21680", 32850, 500)
 {
  Outlier(0.05);
 };
 R_Date("OxA-21584", 32200, 450)
 {
  Outlier(0.05);
 };
 R_Date("OxA-21583", 32400, 450)
 {
  Outlier(0.05);
 };
};
Boundary("Eboulis 6/7");
Boundary("Start 6");
Phase("Niveau 6")
{
 R_Date("OxA-22778", 31850, 450)
 {
  Outlier(0.05);
 };
 R_Date("OxA-21681", 31200, 400)
 {
```

```
   Outlier(0.05);
  };
  R_Date("OxA-21677", 31270, 390)
  {
   Outlier(0.05);
  };
  R_Date("OxA-21676", 31250, 400)
  {
   Outlier(0.05);
  };
 };
 Boundary("Eboulis 5/6");
 Boundary("Start 5");
 Phase("Niveau 5")
 {
  R_Date("OxA-21585", 28180, 270)
  {
   Outlier(0.05);
  };
  R_Date("OxA-21586", 28230, 290)
  {
   Outlier(0.05);
  };
  R_Date("OxA-21587", 28150, 290)
  {
   Outlier(0.05);
  };
  R_Date("OxA-21588", 28250, 280)
  {
   Outlier(0.05);
  };
  R_Date("OxA-X-2225-38", 26780, 280)
  {
   Outlier(0.05);
  };
 };
 Boundary("Eboulis 4/5");
};
Sequence()
{
 Boundary("=Start Eboulis de Base");
 Date("Early Aurignacian");
 Boundary("=Eboulis 8/9");
};
Sequence()
{
 Boundary("=Start 8");
 Date("Evolved Aurignacian");
 Boundary("=Eboulis 5/6");
};
Sequence()
```

```
 {
  Boundary("=Start 5");
  Date("Gravettian");
  Boundary("=Eboulis 4/5");
 };
};
```

Abri Castanet
Abri Castanet is in the Vézère Valley of southwestern France in the Dordogne region. The site has yielded archaeological evidence attributed to the Early Aurignacian. It is dived in two main sectors, North and South. Here is the Bayesian model from White et al. (2012).

Bayesian Modelled Boundaries and Duration of the phases provided by the IntCal13 (Reimer et al., 2013) using OxCal 4.3 (Ramsey, 2009) are the following:

Castanet Northern sector	**Modelled (BP)**			
Indices Amodel 136 Aoverall 138.5	**from**	**to**	**from**	**to**
	68,20%		**95,40%**	
End 1	36230	35590	36410	35030
Early Aurignacian	36430	35860	36940	35410
Start 1	36730	36050	37480	35850
Castanet Southern sector	**Modelled (BP)**			
Indices Amodel 62.5 Aoverall 67.3	**from**	**to**	**from**	**to**
	68,20%		**95,40%**	
End 1	36410	35580	36690	35100
Early Aurignacian	37010	36080	37820	35560
Start 1	37700	36540	38540	36360

In red are the ranges taken for building the bars in the graph in Figure 3 in the main text

CQL Code:

Castanet North

```
Plot()
 {
  Outlier_Model("General",T(5),U(0,4),"t");
  Sequence()
  {
   Boundary("Start 1");
   Phase("1")
   {
    R_Date("OxA-21639", 32900, 500)
    {
     Outlier(0.05);
    };
    R_Date("OxA-21640", 31900, 450)
```

```
    {
     Outlier(0.05);
    };
    R_Date("OxA-21641*", 31950, 450)
    {
     Outlier(0.05);
    };
    R_Date("OxA-21642*", 32500, 450)
    {
     Outlier(0.05);
    };
    R_Date("OxA-21643", 32200, 450)
    {
     Outlier(0.05);
    };
    R_Date("OxA-21644", 32350, 450)
    {
     Outlier(0.05);
    };
    R_Date("OxA-21645", 32000, 450)
    {
     Outlier(0.05);
    };
   };
   Boundary("End 1");
  };
  Sequence()
  {
   Boundary("=Start 1");
   Date("Early Aurignacian");
   Boundary("=End 1");
  };
 };
```

Castanet South

```
Plot()
 {
  Outlier_Model("General",T(5),U(0,4),"t");
  Sequence()
  {
   Boundary("Start 1");
   Phase("1")
   {
    R_Date("OxA-21558", 32350, 450)
    {
     Outlier(0.05);
    };
    R_Date("OxA-21559", 33250, 500)
    {
     Outlier(0.05);
    };
```

```
  R_Date("OxA-21560", 32800, 450)
  {
   Outlier(0.05);
  };
  R_Date("OxA-21561", 32050, 450)
  {
   Outlier(0.05);
  };
  R_Date("OxA-21562", 32550, 450)
  {
   Outlier(0.05);
  };
  R_Date("OxA-21563", 32600, 450)
  {
   Outlier(0.05);
  };
  R_Date("OxA-21564", 32950, 500)
  {
   Outlier(0.05);
  };
  R_Date("OxA-21566", 32550, 600)
  {
   Outlier(0.05);
  };
  R_Date("GifA-97313", 32750, 460)
  {
   Outlier(0.05);
  };
  R_Date("GifA-97312", 32460, 420)
  {
   Outlier(0.05);
  };
  R_Date("GifA-99166", 34320, 520)
  {
   Outlier(0.05);
  };
  R_Date("GifA-99165", 31430, 390)
  {
   Outlier(0.05);
  };
  R_Date("GifA-99179", 32310, 520)
  {
   Outlier(0.05);
  };
  R_Date("GifA-99180", 32950, 520)
  {
   Outlier(0.05);
  };
 };
 Boundary("End 1");
};
```

```
 Sequence()
 {
  Boundary("=Start 1");
  Date("Early Aurignacian");
  Boundary("=End 1");
 };
};
```

Abri Cellier:
Abri Cellier is a rock shelter on the right bank of the Vézère River in southwestern France. The site has yielded archaeological evidence attributed to Upper Palaeolithic with different Aurignacian levels. The Bayesian model is taken from White et al. (2018).

Bayesian Modelled Boundaries and Duration of the phases provided by the IntCal13 (Reimer et al., 2013) using OxCal 4.3 (Ramsey, 2009) are the following:

Abtri Cellier	**Modelled (BP)**			
Indices Amodel 28.7 Aoverall 29.9	**from**	**to**	**from**	**to**
	68,20%		**95,40%**	
End 100	32650	30500	36150	27450
Aurignacian?	33300	31200	36180	30220
Start 100	34160	31710	36150	31560
End 102	36550	34680	36940	32830
Recent Aurignacian	36740	35400	37360	34020
Start 102	36990	35960	37680	35470
End 104	37560	36450	38170	36060
Early Aurignacian	37940	36690	38670	36260
Start 104	38400	36870	39310	36390

In red are the ranges taken for building the bars in the graph in Figure 3 in the main text

CQL Code:

```
Plot()
 {
  Outlier_Model("General",T(5),U(0,4),"t");
  Sequence()
  {
   Boundary("Start 104");
   Phase("104")
   {
    R_Date("OxA-32204", 33600, 550)
    {
     Outlier(0.05);
```

```
   };
   R_Date("OxA-32201", 32650, 500)
   {
    Outlier(0.05);
   };
   R_Date("OxA-32202", 28330, 290)
   {
    Outlier(0.05);
   };
  };
  Boundary("End 104");
  Boundary("Start 102");
  Phase("102")
  {
   R_Date("OxA-32203", 32450, 450)
   {
    Outlier(0.05);
   };
  };
  Boundary("End 102");
  Boundary("Start 100");
  Phase("100")
  {
   R_Date("OxA-X-2628-42", 28060, 310)
   {
    Outlier(0.05);
   };
  };
  Boundary("End 100");
 };
 Sequence()
 {
  Boundary("=Start 104");
  Date("Early Aurignacian");
  Boundary("=End 104");
 };
 Sequence()
 {
  Boundary("=Start 102");
  Date("Recent Aurignacian");
  Boundary("=End 102");
 };
 Sequence()
 {
  Boundary("=Start 100");
  Date("Aurignacian?");
  Boundary("=End 100");
 };
};
```

Abri Blanchard
Very close to Castanet is the site of Abri Blanchard, a partially collapsed rock shelter situated in the Vézère Valley of the Dordogne region of southwestern France. Is a major site for understanding the Aurignacian, with two archaeological units attributed to Early and/or Aurignacian (Layer B and D). The dates published in Bourrillon et al. (2018) belong to the Early Aurignacian Sector 4/5 and are based on hydroxyproline (Hyp) AMS radiocarbon date. Here we build a Bayesian model based on the two dates to understand the duration of Sector 4/5, the only Upper Palaeolithic level.

Bayesian Modelled Boundaries and Duration of the phase provided by the IntCal13 (Reimer et al., 2013) using OxCal 4.3 (Ramsey, 2009) are the following:

Abtri Blanchard	**Modelled (BP)**			
Indices Amodel 101 Aoverall 102.1	**from**	**to**	**from**	**to**
	68,20%		**95,40%**	
End Early Aurignacian	38440	36020	38580	30110
Early Aurignacian	39130	36930	42470	33760
Start Early Aurignacian	40200	37690	46340	37420

In red are the ranges taken for building the bars in the graph in Figure 3 in the main text

CQL Code:

```
Plot()
 {
  Outlier_Model("General",T(5),U(0,4),"t");
  Sequence()
  {
   Boundary("Start Early Aurignacian");
   Phase("1")
   {
    R_Date("OxA-X-2669-54", 33420, 350)
    {
     Outlier(0.05);
    };
    R_Date("OxA-X-2669-55", 33960, 360)
    {
     Outlier(0.05);
    };
   };
   Boundary("End Early Aurignacian");
  };
  Sequence()
  {
   Boundary("=Start Early Aurignacian");
   Date("Early Aurignacian");
   Boundary("=End Early Aurignacian");
  };
 };
```

Rhône-Alpes region

Grotte Mandrin

Grotte Mandrin is a rock shelter located in the Middle Rhône valley. There exist several Mousterian levels interstratified with Neronian assemblages and ending with the Protoaurignacian. We used the Bayesian model in Higham et al. (2014). However, the Neronian phase is present in the model without any dates, so even in this case, the duration range of the Neronian could be considered as an 'artificial' boundary.

Bayesian Modelled Boundaries and Duration of the phases provided by the IntCal13 (Reimer et al., 2013) using OxCal 4.3 (Ramsey, 2009) are the following:

Grotte Mandrin	**Modelled (BP)**			
Indices Amodel 25.9 Aoverall 15.6	**from**	**to**	**from**	**to**
	68,20%		**95,40%**	
B1/Sterile level	44260	43010	44290	40930
Phase III Post-Neronian	46820	43690	50160	42380
Neronian/D post-Neronian I	49280	45520	52400	44910
Neronian/D post-Neronian I	49280	45520	52400	44910
Phase II Neronian	49890	45750	53170	45150
F Quina/E Neronian	50430	45930	54020	45390
F Quina/E Neronian	50430	45930	54020	45390
Mousterian	51070	46150	54700	45640
G Ferrassie/F Quina	51740	46340	55530	45900
G Ferrassie/F Quina	51740	46340	55530	45900
Mousterian Ferrassie	52600	46520	56530	46240
Start G Ferrassie	53980	...	57440	...

In red are the ranges taken for building the bars in the graph in Figure 3 in the main text

CQL Code:

```
Options()
 {
  Resolution=20;
  Plot()
  {
   Outlier_Model("General",T(5),U(0,4),"t");
   Sequence()
   {
    Boundary("Start G Ferrassie");
    Phase("G Ferrassie Mousterian")
    {
     Age("TL ave", N(52000,3350))
     {
```

```
  Outlier(0.05);
 };
};
Boundary("G Ferrassie/F Quina");
Phase("Phase I layer F Quina")
{
};
Boundary("F Quina/E Neronian");
Phase("Phase II Layer E Neronian")
{
 Date("Neronian");
};
Boundary("Neronian/D post-Neronian I");
Phase("Phase III layer D post Neronian I")
{
};
Boundary("End of D post-Neronian I");
Boundary("Transition D/C");
Phase("C post-Neronian II")
{
 R_F14C("OxA-X-2286-14", 0.00485, 0.00108)
 {
  Outlier(0.05);
 };
 R_F14C("OxA-X-2286-13", 0.00463, 0.00113)
 {
  Outlier(0.05);
 };
};
Boundary("C end/start sterile");
Boundary("End sterile/start B post-Neronian II");
Phase("post-Neronian II")
{
 R_F14C("OxA-22120", 0.00448, 0.00102)
 {
  Outlier(0.05);
 };
 R_F14C("OxA-21685", 0.00781, 0.001)
 {
  Outlier(0.05);
 };
 R_F14C("OxA-X-2286-10", 0.00832, 0.00101)
 {
  Outlier(0.05);
 };
 Age("TL ave", N(35000,1600))
 {
  Outlier(0.05);
 };
 R_F14C("OxA-21690", 0.0056, 0.00098)
 {
```

```
    Outlier(0.05);
   };
   R_F14C("OxA-22121", 0.00666, 0.00098)
   {
    Outlier(0.05);
   };
   R_F14C("OxA-21691", 0.00354, 0.00096)
   {
    Outlier(0.05);
   };
  };
  Boundary("B1/Sterile level");
  Boundary("Start Layer B1");
  Phase("Phase IV Layer B1 ProtoAurignacian Level 1")
  {
  };
  Boundary("End Layer B1");
 };
 Sequence()
 {
  Boundary("=Start G Ferrassie");
  Date("Mousterian Ferrassie");
  Boundary("=G Ferrassie/F Quina");
 };
 Sequence()
 {
  Boundary("=G Ferrassie/F Quina");
  Date("Mousterian");
  Boundary("=F Quina/E Neronian");
 };
 Sequence()
 {
  Boundary("=F Quina/E Neronian");
  Date("Phase II Neronian");
  Boundary("=Neronian/D post-Neronian I");
 };
 Sequence()
 {
  Boundary("=Neronian/D post-Neronian I");
  Date("Phase III Post-Neronian");
  Boundary("=B1/Sterile level");
 };
 Sequence()
 {
  Boundary("=Start Layer B1");
  Date("ProtoAurignacian");
  Boundary("=End Layer B1");
 };
};
};
```

Saint Marcel
The site is situated at the end of the Ardèche Gorge in Rhône-Alpes region. It yielded only Middle Palaeolithic. In Szmidt et al. (2010a) there are three radiocarbon dates from Layer F. We built a model only to obtain the boundaries of this layer.

Bayesian Modelled Boundaries and Duration of the phase provided by the IntCal13 (Reimer et al., 2013) using OxCal 4.3 (Ramsey, 2009) are the following:

Saint Marcel Cave	**Modelled (BP)**			
Indices Amodel 89 Aoverall 90.5	**from**	**to**	**from**	**to**
	68,20%		**95,40%**	
End Mousterian	42560	40510	42910	34720
Mousterian	44040	41410	48970	37780
Start Mousterian	45770	42130	52920	41850

In red are the ranges taken for building the bars in the graph in Figure 3 in the main text

CQL Code:

```
Plot()
 {
  Outlier_Model("General",T(5),U(0,4),"t");
  Sequence("Saint Marcel Cave")
  {
   Boundary("Start Mousterian");
   Phase("1")
   {
    R_Date("OxA-19623", 37850, 550)
    {
     Outlier(0.05);
    };
    R_Date("OxA-19624", 41300, 1700)
    {
     Outlier(0.05);
    };
    R_Date("OxA-19625", 37850, 600)
    {
     Outlier(0.05);
    };
   };
   Boundary("End Mousterian");
  };
  Sequence()
  {
   Boundary("=Start Mousterian");
   Date("Mousterian");
   Boundary("=End Mousterian");
```

};
};

Centre region

Roches d'Abilly
Les Roches d'Abilly is located in central France midway between Saint Césaire and the Grotte du Renne, Arcy-sur-Cure. The archaeological layers are subdivided in Mousterian Levallois, Mousterian Discoidal, the Châtelperronian and the final Aurignacian phase. We built a Bayesian model modifying the one published in Aubry et al. (2014). We inserted the correct ^{14}C result from Beta Analytic (Beta-249596 ^{14}C Age 35,770±380) in the layer E. In fact, we noticed that the Bayesian model of Aubry et al. (2014) is Beta-234192, which does not correspond to the right number in Aubry et al. 2012 (Beta-234193 ^{14}C Age 31,640±230). This later one is the Layer F and not the one for Layer E. The OSL determinations are taken from Table 3 in Thomsen et al. (2016). In this table, the new OSL determination (OSL-092201=46,100±2400) is somehow older than the one proposed previously in Aubry et al. (2014) (OSL-092201=43,700±2200), this latter one looks more coherent with the stratigraphy.

Bayesian Modelled Boundaries and Duration of the phases provided by the IntCal13 (Reimer et al., 2013) using OxCal 4.3 (Ramsey, 2009) are the following:

Roches d'Abilly	**Modelled (BP)**			
Indices Amodel 72 Aoverall 74.9	**from**	**to**	**from**	**to**
	68,20%		**95,40%**	
End Aurignacian	40740	38910	41220	36640
Aurignacian	41180	39710	42100	38170
Transition Phase CP/Aurignacian	41700	40320	42570	39860
Transition Phase CP/Aurignacian	41700	40320	42570	39860
Châtelperronian	43250	41420	44050	40610
Transition Phase Discoide/Phase CP	44300	42930	44850	42170
Transition Phase Discoide/Phase CP	44300	42930	44850	42170
Discoide Mousterian	44680	43420	45440	42770
Transition Phase Levallois/Phase Discoide	45220	43810	46090	43290
Transition Phase Levallois/Phase Discoide	45220	43810	46090	43290
Mousterian Levallois	46010	44040	48220	43380
Start Levallois	47000	44130	50330	43450

In red are the ranges taken for building the bars in the graph in Figure 3 in the main text

CQL Code:

```
Plot()
 {
  Outlier_Model("General",T(5),U(0,4),"t");
  Sequence()
  {
   Boundary("Start Levallois");
   Phase("3")
   {
    R_Date("OxA-29527", 41900, 1500)
    {
     Outlier(0.05);
    };
   };
   Boundary("Transition Phase Levallois/Phase Discoide");
   Phase("4")
   {
    R_Date("OxA-22316", 41200, 1300)
    {
     Outlier(0.05);
    };
    R_Date("OxA-26471", 41000, 1300)
    {
     Outlier(0.05);
    };
    R_Date("OxA-26472", 40600, 1200)
    {
     Outlier(0.05);
    };
    R_Date("OxA-26470", 39100, 1000)
    {
     Outlier(0.05);
    };
    Age("OSL-092201 Quartz", N(46100,2400))
    {
     Outlier(0.05);
    };
   };
   Boundary("Transition Phase Discoide/Phase CP");
   Phase("5")
   {
    R_Date("OxA-22342", 37400, 800)
    {
     Outlier(0.05);
    };
    Age("OSL-092202 Quartz", N(42400,2300))
    {
     Outlier(0.05);
    };
    Age("OSL-092202 Feld", N(46900,1900))
```

```
   {
    Outlier(0.05);
   };
  };
  Boundary("Transition Phase CP/Aurignacian");
  Phase("6")
  {
   R_Date("Lyon-6920", 34520, 850)
   {
    Outlier(0.05);
   };
   R_Date("Beta-249596", 35770, 380)
   {
    Outlier(0.05);
   };
  };
  Boundary("End Aurignacian");
 };
 Sequence()
 {
  Boundary("=Start Levallois");
  Date("Mousterian Levallois");
  Boundary("=Transition Phase Levallois/Phase Discoide");
 };
 Sequence()
 {
  Boundary("=Transition Phase Levallois/Phase Discoide");
  Date("Discoide Mousterian");
  Boundary("=Transition Phase Discoide/Phase CP");
 };
 Sequence()
 {
  Boundary("=Transition Phase Discoide/Phase CP");
  Date("CP");
  Boundary("=Transition Phase CP/Aurignacian");
 };
 Sequence()
 {
  Boundary("=Transition Phase CP/Aurignacian");
  Date("Aurignacian");
  Boundary("=End Aurignacian");
 };
};
```

Les Cottés

Les Cottés is located on the edge of the Seuil du Poitou and the Touraine, on the border of the department of Vienne, in the Central region. The archaeological layers are from the Mousterian, Châtelperronian, Protoaurignacian and at the top, the Early Aurignacian all separated by sterile layers. The Bayesian model is reproduced from the publication of Talamo et al. (2012).

Bayesian Modelled Boundaries and Duration of the phases provided by the IntCal13 (Reimer et al., 2013) using OxCal 4.3 (Ramsey, 2009) are the following:

Les Cottés	**Modelled (BP)**			
Indices Amodel 68.1 Aoverall 70.4	**from**	**to**	**from**	**to**
	68,20%		**95,40%**	
End Early Aurignacian US2	36020	35180	36300	34380
Early Aurignacian	37930	35980	38540	35270
Start Early Aurignacian US4 Upper	38670	38060	38940	37670
End Protoaurignacian US4 Lower	39000	38490	39250	38190
Protoaurignacian	39340	38740	39910	38440
Start Protoaurignacian US4 Lower	39730	38940	40420	38790
End Châtelperronian	41240	40300	42390	39540
Châtelperronian	42480	41210	42770	40430
Start Châtelperronian	42780	42360	43050	42200
End Mousterian	43090	42580	43430	42370
Mousterian	45150	43230	45810	42710
Start Mousterian	45950	45150	46680	44870

In red are the ranges taken for building the bars in the graph in Figure 3 in the main text

CQL Code:

```
Plot()
 {
  Outlier_Model("General",T(5),U(0,4),"t");
  Sequence("Les Cottes")
  {
   Boundary("Start Mousterian");
   Phase("Mousterian")
   {
    R_Date("S-EVA 13676", 42180, 280)
    {
     Outlier(0.05);
    };
    R_Date("S-EVA 13675", 41640, 260)
    {
     Outlier(0.05);
    };
    R_Date("S-EVA 13673", 39760, 1600)
    {
     Outlier(0.05);
    };
```

```
 R_Date("S-EVA 13679", 39390, 470)
 {
  Outlier(0.05);
 };
 R_Date("S-EVA 13677", 39260, 770)
 {
  Outlier(0.05);
 };
 R_Date("S-EVA 13678", 38970, 440)
 {
  Outlier(0.05);
 };
};
Boundary("End Mousterian");
Boundary("Start Chatelperronian");
Phase("Chatelperronian")
{
 R_Date("S-EVA 9695", 38540, 270)
 {
  Outlier(0.05);
 };
 R_Date("S-EVA 13668", 38100, 210)
 {
  Outlier(0.05);
 };
 R_Date("S-EVA 13667", 37360, 610)
 {
  Outlier(0.05);
 };
 R_Date("S-EVA 13666", 36230, 210)
 {
  Outlier(0.05);
 };
};
Boundary("End Chatelperronian");
Boundary("Start Protoaurignacian US04 Lower");
Phase("Protoaurignacian US04 Lower")
{
 R_Date("S-EVA 9713", 35150, 280)
 {
  Outlier(0.05);
 };
 R_Date("S-EVA 13665", 34620, 390)
 {
  Outlier(0.05);
 };
 R_Date("S-EVA 13669", 34430, 180)
 {
  Outlier(0.05);
 };
 R_Date("S-EVA 13672", 34080, 250)
```

```
  {
   Outlier(0.05);
  };
 };
 Boundary("End Protoaurignacian US04 Lower");
 Boundary("Start Early Aurignacian US04 Upper");
 Phase("Early Aurignacian US04 Upper")
 {
  R_Date("S-EVA 9720", 33860, 160)
  {
   Outlier(0.05);
  };
  R_Date("S-EVA 9711", 33180, 160)
  {
   Outlier(0.05);
  };
 };
 Boundary("End Early Aurignacian US04 Upper");
 Boundary("Start Early Aurignacian US02");
 Phase(" Early Aurignacian US02")
 {
  R_Date("S-EVA 9719", 32670, 120)
  {
   Outlier(0.05);
  };
  R_Date("S-EVA 9718", 31810, 250)
  {
   Outlier(0.05);
  };
  R_Date("S-EVA 9717", 31750, 280)
  {
   Outlier(0.05);
  };
 };
 Boundary("End Early Aurignacian US02");
};
Sequence()
{
 Boundary("=Start Mousterian");
 Date("Mousterian");
 Boundary("=End Mousterian");
};
Sequence()
{
 Boundary("=Start Chatelperronian");
 Date("Chatelperronian");
 Boundary("=End Chatelperronian");
};
Sequence()
{
 Boundary("=Start Protoaurignacian US04 Lower");
```

```
 Date("Protoaurignacian");
 Boundary("=End Protoaurignacian US04 Lower");
};
Sequence()
{
 Boundary("=Start Early Aurignacian US04 Upper");
 Date("Protoaurignacian");
 Boundary("=End Early Aurignacian US02");
};
};
```

Bourgogne region

Grotte du Renne (Arcy-sur-Cure)

The Grotte du Renne at Arcy-sur-Cure is located in the Yonne department in northern Burgundy region of France. The site is one of several caves in an integrated karst system and has yielded archaeological evidence for Mousterian, Châtelperronian, and Protoaurignacian at the top. Grotte du Renne has been a very controversial site, studied in different ways. The studies by Welker et al. (2016) and Hublin et al. (1996, 2012) showed that Neandertals made the Châtelperronian. Here we report two different Bayesian models, the one in Welker et al. (2016) (with an Overall Agreement of 64.9%) and the one by Higham et al. (2014) (with an Overall Agreement of 3.2%). We decided to run the two different models because there are different ranges of the Protoaurignacian and to show that the different models lead to the same time span for the Châtelperronian and the Mousterian.

Bayesian Modelled Boundaries and Duration of the phases provided by the IntCal13 (Reimer et al., 2013) using OxCal 4.3 (Ramsey, 2009) are the following:

Grotte du Renne_Welker et al. 2014	**Modelled (BP)**			
Indices Amodel 61.5 Aoverall 64.9	**from**	**to**	**from**	**to**
	68,20%		**95,40%**	
Transition Mousterian XI/CP Layer IX+X	44700	44100	45030	43850
Mousterian	45710	44450	46980	44080
Start Mousterian XI	46780	45100	48250	44610
Transition CP VIII/Proto VII	40950	39990	41150	39380
Châtelperronian	43920	41060	44530	40220
Transition Mousterian XI/CP Layer IX+X	44700	44100	45030	43850
End ProtoAurignacian VII	34230	32760	35340	30480
Protoaurignacian	39500	34240	40670	33010
Transition CP VIII/Proto VII	40950	39990	41150	39380
Grotte du Renne_Higham et al. 2014	**Modelled (BP)**			

Indices Amodel 2.5 Aoverall 3.2	**from**	**to**	**from**	**to**
	68,20%		**95,40%**	
end XI/Start X	44840	44190	45180	43850
Arcy Mousterian	45450	44370	46860	43940
XII	46160	44610	48330	44220
VIII/VII	40700	39670	41370	39300
Arcy Châtelperronian	44040	41100	44610	40110
end XI/Start X	44840	44190	45180	43850
VII/VI	39750	38320	40200	37180
Arcy Protoaurignacian	40200	39030	40880	38150
VIII/VII	40700	39670	41370	39300

In red are the ranges taken for building the bars in the graph in Figure 3 in the main text

CQL Code:

```
Plot()
 {
  Outlier_Model("General",T(5),U(0,4),"t");
  Sequence(Grotte du Renne_Welker et al. 2016)
  {
   Boundary("Start Mousterian XI");
   Phase("Mousterian XI")
   {
    R_Date("EVA-84", 43266, 929)
    {
     Outlier(0.05);
    };
    R_Date("EVA-77", 42122, 805)
    {
     Outlier(0.05);
    };
    R_Date("EVA-83", 41979, 821)
    {
     Outlier(0.05);
    };
    R_Date("EVA-85", 40898, 719)
    {
     Outlier(0.05);
    };
   };
   Boundary("Transition Mousterian XI/CP Layer IX+X");
   Phase("Chatelperronian Layer")
   {
    R_Date("EVA-33", 40968, 424)
```

```
{
 Outlier(0.05);
};
R_Date("EVA-28", 40925, 393)
{
 Outlier(0.05);
};
R_Date("EVA-49", 40834, 778)
{
 Outlier(0.05);
};
R_Date("EVA-34", 40519, 389)
{
 Outlier(0.05);
};
R_Date("EVA-27", 40231, 395)
{
 Outlier(0.05);
};
R_Date("EVA-51", 39958, 702)
{
 Outlier(0.05);
};
R_Date("EVA-46", 39932, 361)
{
 Outlier(0.05);
};
R_Date("EVA-47", 39754, 360)
{
 Outlier(0.05);
};
R_Date("EVA-37", 39448, 340)
{
 Outlier(0.05);
};
R_Date("EVA-26", 39393, 334)
{
 Outlier(0.05);
};
R_Date("EVA-31", 39290, 334)
{
 Outlier(0.05);
};
R_Date("EVA-44", 39277, 351)
{
 Outlier(0.05);
};
R_Date("EVA-35", 39243, 341)
{
 Outlier(0.05);
};
```

```
R_Date("EVA-48", 39071, 332)
{
 Outlier(0.05);
};
R_Date("EVA-43", 39015, 352)
{
 Outlier(0.05);
};
R_Date("EVA-41", 38733, 333)
{
 Outlier(0.05);
};
R_Date("EVA-24", 38395, 317)
{
 Outlier(0.05);
};
R_Date("EVA-42", 38065, 311)
{
 Outlier(0.05);
};
R_Date("EVA-30", 37984, 284)
{
 Outlier(0.05);
};
R_Date("EVA-36", 37742, 307)
{
 Outlier(0.05);
};
R_Date("EVA-40", 37512, 275)
{
 Outlier(0.05);
};
R_Date("MAMS-25149", 36840, 660)
{
 color="red";
 fill="red";
 Outlier(0.05);
};
R_Date("EVA-23", 36837, 335)
{
 Outlier(0.05);
};
R_Date("EVA-32", 36815, 257)
{
 Outlier(0.05);
};
R_Date("EVA-38", 36536, 248)
{
 Outlier(0.05);
};
R_Date("EVA-25", 36207, 250)
```

```
 {
  Outlier(0.05);
 };
 R_Date("EVA-29", 35498, 216)
 {
  Outlier(1.0);
 };
};
Boundary("Transition CP Layer IX+X/VIII");
Phase("Chatelperronian Layer VIII")
{
 R_Date("EVA-56", 37712, 533)
 {
  Outlier(0.05);
 };
 R_Date("EVA-55", 36626, 452)
 {
  Outlier(0.05);
 };
 R_Date("EVA-53", 36232, 435)
 {
  Outlier(0.05);
 };
 R_Date("EVA-52", 35984, 432)
 {
  Outlier(0.05);
 };
 R_Date("EVA-54", 35379, 390)
 {
  Outlier(0.05);
 };
};
Boundary("Transition CP VIII/Proto VII");
Phase("Protoaurignacian VII")
{
 R_Date("EVA-95", 34807, 210)
 {
  Outlier(0.05);
 };
 R_Date("EVA-81", 33849, 311)
 {
  Outlier(0.05);
 };
 R_Date("EVA-93", 33007, 182)
 {
  Outlier(0.05);
 };
 R_Date("EVA-92", 31610, 185)
 {
  Outlier(0.05);
 };
```

```
   R_Date("EVA-79", 29934, 208)
   {
    Outlier(0.05);
   };
  };
  Boundary("End Protoaurignacian VII");
 };
 Sequence()
 {
  Boundary("=Transition CP VIII/Proto VII");
  Date("Protoaurignacian");
  Boundary("=End Protoaurignacian VII");
 };
 Sequence()
 {
  Boundary("=Transition Mousterian XI/CP Layer IX+X");
  Date("Chatelperronian");
  Boundary("=Transition CP VIII/Proto VII");
 };
 Sequence()
 {
  Boundary("=Start Mousterian XI");
  Date("Mousterian");
  Boundary("=Transition Mousterian XI/CP Layer IX+X");
 };
};

Plot()
{
 Outlier_Model("General",T(5),U(0,4),"t");
 Sequence(Grotte du Renne_Higham et al. 2014)
 {
  Boundary("XII");
  Phase("XII Mousterian")
  {
   R_F14C("OxA-21594",0.00996,0.00126)
   {
    Outlier("General", 0.05);
   };
   R_F14C("OxA-21595",0.00862,0.00127)
   {
    Outlier("General", 0.05);
   };
  };
  Boundary("Start XI");
  Phase("XI Mousterian")
  {
   R_Date("EVA-77*", 42120, 805)
   {
    Outlier("General", 0.05);
   };
```

```
 R_Date("EVA-83*", 41980, 821)
 {
  Outlier("General", 0.05);
 };
 R_Date("EVA-85*", 40900, 719)
 {
  Outlier("General", 0.05);
 };
};
Boundary("end XI/Start X");
Phase("X + IX Chatelperronian")
{
 R_Date("EVA-30*", 37980, 284)
 {
  Outlier("General", 0.05);
 };
 R_Date("EVA-29*", 35500, 216)
 {
  Outlier("General", 0.05);
 };
 R_Date("EVA-26*", 39390, 334)
 {
  Outlier("General", 0.05);
 };
 R_Date("EVA-42*", 38070, 311)
 {
  Outlier("General", 0.05);
 };
 R_Date("EVA-41*", 38730, 333)
 {
  Outlier("General", 0.05);
 };
 R_F14C("OxA-21576",0.00621,0.00131)
 {
  Outlier("General", 0.05);
 };
 R_F14C("OxA-21577",0.01338,0.00132)
 {
  Outlier("General", 0.05);
 };
 R_Date("OxA-21590",21150,160)
 {
  Outlier("General", 1.00);
 };
 R_F14C("OxA-21591",0.0132,0.00126)
 {
  Outlier("General", 0.05);
 };
 R_F14C("OxA-21565",0.00895,0.00099)
 {
  Outlier("General", 0.05);
```

```
};
R_F14C("OxA-21593",0.01231,0.00132)
{
 Outlier("General", 0.05);
};
R_F14C("OxA-X-2279-18",0.00639,0.001)
{
 Outlier("General", 0.05);
};
R_F14C("OxA-X-2279-45",0.00618,0.00102)
{
 Outlier("General", 0.05);
};
R_F14C("OxA-X-2279-46",0.00807,0.001)
{
 Outlier("General", 0.05);
};
R_Date("OxA-X-2222-21", 23120, 190)
{
 Outlier("General", 1.00);
};
R_F14C("OxA-X-2226-7",0.0083,0.00134)
{
 Outlier("General", 0.05);
};
R_F14C("OxA-21577",0.01338,0.00132)
{
 Outlier("General", 0.05);
};
R_F14C("OxA-21592",0.01102,0.00149)
{
 Outlier("General", 0.05);
};
R_F14C("OxA-X-2226-12",0.0057,0.00137)
{
 Outlier("General", 0.05);
};
R_F14C("OxA-X-2226-13",0.00782,0.00136)
{
 Outlier("General", 0.05);
};
R_F14C("OxA-X-2279-44",0.00233,0.00104)
{
 Outlier("General", 0.05);
};
R_Date("EVA-34*", 40520, 389)
{
 Outlier("General", 0.05);
};
R_Date("EVA-33*", 40970, 424)
{
```

```
  Outlier("General", 0.05);
 };
 R_F14C("OxA-21574",0.00794,0.00127)
 {
  Outlier("General", 0.05);
 };
 R_F14C("OxA-21575",0.01837,0.00129)
 {
  Outlier("General", 0.05);
 };
};
Boundary("end X/Start IX");
Phase("VIII")
{
 R_Date("EVA-56*", 37710, 533)
 {
  Outlier("General", 0.05);
 };
 R_Date("EVA-55*", 36630, 452)
 {
  Outlier("General", 0.05);
 };
 R_F14C("OxA-21573",0.01018,0.0013)
 {
  Outlier("General", 0.05);
 };
 R_F14C("OxA-X-2279-14",0.01215,0.00112)
 {
  Outlier("General", 0.05);
 };
 R_F14C("OxA-21683",0.00684,0.00099)
 {
  Outlier("General", 0.05);
 };
};
Boundary("VIII/VII");
Phase("VII Aurignacian")
{
 R_F14C("OxA-21569",0.01062,0.00166)
 {
  Outlier("General", 0.05);
 };
 R_F14C("OxA-21570",0.01347,0.00137)
 {
  Outlier("General", 0.05);
 };
 R_F14C("OxA-21571",0.01444,0.00132)
 {
  Outlier("General", 0.05);
 };
 R_F14C("OxA-21572",0.01343,0.00127)
```

```
   {
    Outlier("General", 0.05);
   };
   R_F14C("OxA-21682",0.0128,0.001)
   {
    Outlier("General", 0.05);
   };
  };
  Boundary("VII/VI");
 };
 Sequence()
 {
  Boundary("=VIII/VII");
  Date("Arcy Protoaurignacian");
  Boundary("=VII/VI");
 };
 Sequence()
 {
  Boundary("=end XI/Start X");
  Date("Arcy Chatelperronian");
  Boundary("=VIII/VII");
 };
 Sequence()
 {
  Boundary("=XII");
  Date("Arcy Mousterian");
  Boundary("=end XI/Start X");
 };
};
```

Verpillière I and Solutré
Verpillière I and Solutré are located in the Saône-et-Loire region of southern Burgundy. Verpillière I has yielded archaeological evidence from the Middle Palaeolithic to the Gravettian with, Châtelperronian, and Aurignacian (Floss et al., 2016). Solutré is an Aurignacian site (Floss et al., 2015).

Here we reported both sites on the map, but we did not do a Bayesian analysis or calibration since in the paper of Floss et al. (2015) it is mentioned that the dating program is underway.

Trou de la Mère Clochette (TMC)
The site is located close to Verpillière I and Solutré, in the Saône-et-Loire region southern Burgundy. It is a very important site for the presence and the direct date of split-based points. Two radiocarbon dates have been published in Szmidt et al. (2010b) from Unit C. This Unit has yielded Upper Palaeolithic (Proto- and Early Aurignacian) industry together with Neolithic human remains. Here we make a simple Bayesian model based on just these two dates to indicate the range of Unit C.

Bayesian Modelled Boundaries and Duration of Unit C provided by the IntCal13 (Reimer et al., 2013) using OxCal 4.3 (Ramsey, 2009) are the following:

TMC	**Modelled (BP)**			
Indices Amodel 99.7 Aoverall 99.6	**from**	**to**	**from**	**to**
	68,20%		**95,40%**	
End Unit C	38750	30060	38910	30060
Unit C	41220	37040	44720	33280
Start Unit C	47480	39620	47490	39550

In red are the ranges taken for building the bars in the graph in Figure 3 in the main text

CQL Code:

```
Plot()
 {
  Outlier_Model("General",T(5),U(0,4),"t");
  Sequence()
  {
   Boundary("Start Unit C");
   Phase("Unit C")
   {
    R_Date("TMC-CFer-OxA- 19622", 35460, 250)
    {
     Outlier(0.05);
    };
    R_Date("TMC-CFer-OxA- 19621", 33750, 350)
    {
     Outlier(0.05);
    };
   };
   Boundary("End Unit C");
  };
  Sequence()
  {
   Boundary("=Start Unit C");
   Date("Unit C");
   Boundary("=End Unit C");
  };
 };
```

<u>Aquitaine region</u>
Isturitz
Isturitz is located in the very southwestern part of the Aquitaine region in south-western France. It is a large cave composed of different chambers, most of them have yielded archaeological sequences of Aurignacian (Protoaurignacian and Early Aurignacian). Here we reproduced the Bayesian model in Barshay-Szmidt et al. (2018a).

Some concerns need to be raised as to why the Bayesian model places Isturitz's earliest Protoaurignacian, level C4d, in the 42-41.5 ka interval. One aspect is the constraint imposed by the modelled results for overlying level C4c, based on six dates of lab AA with errors between 720 and 3600 years, The same lab dated two samples of level 4d, >38k ^{14}C BP and 40.000 +- 2800 ^{14}C BP. Clearly, the uncertainties associated with this lab's results ought to recommend caution in using them. If we only consider the OxA results for layer 4d we see that they return calibrated ages ranging from 40.1 to 43.3 ka cal BP. Ignoring the AA dates of huge uncertainties the chronology of Isturitz's layer C4d is entirely consistent with an age of ca. 40.0-41.5 ka cal BP age as for the Protoaurignacian elsewhere in Europe.

Bayesian Modelled Boundaries and Duration of the phases provided by the IntCal13 (Reimer et al., 2013) using OxCal 4.3 (Ramsey, 2009) are the following:

Isturitz	**Modelled (BP)**			
Indices Amodel 149 Aoverall 140	**from**	**to**	**from**	**to**
	68,20%		**95,40%**	
End Early Aurignacian C 4b1	39770	38900	40150	38360
Early Aurignacian	39890	39160	40250	38750
Transition Proto+Auri C 4b2/Early Aurignacian C 4b1	40060	39390	40390	39060
Transition Proto+Auri C 4b2/Early Aurignacian C 4b1	40060	39390	40390	39060
Proto+Auri	41340	40050	41760	39550
Transition Protoaurignacian C 4d1/Proto+Auri C 4c4	41900	41360	42140	41040
Transition Protoaurignacian C 4d1/Proto+Auri C 4c4	41900	41360	42140	41040
Only Protoaurignacian	42080	41500	42450	41170
Start Protoaurignacian C 4d1	42300	41590	42840	41260

In red are the ranges taken for building the bars in the graph in Figure 3 in the main text

CQL Code:

```
Plot()
 {
  Outlier_Model("General",T(5),U(0,4),"t");
  Sequence()
  {
   Boundary("Start Protoaurignacian C 4d1");
   Phase("C 4d1")
   {
    R_Date("C4d1c-AA-69187", 40000, 2800)
    {
     Outlier(0.05);
    };
    R_Date("C4d1j OxA-23435", 37500, 900)
    {
```

```
  Outlier(0.05);
 };
 R_Date("C4d1j-OxA-23436", 37400, 900)
 {
  Outlier(0.05);
 };
 R_Date(" C4d1j OxA-23434", 37000, 800)
 {
  Outlier(0.05);
 };
 R_Date("C4d1j-OxA-23432-33", 37000, 566)
 {
  Outlier(0.05);
 };
};
Boundary("Transition Protoaurignacian C 4d1/Proto+Auri C 4c4");
Phase("C 4c4")
{
 R_Date("C4c4-AA-69184", 40200, 3600)
 {
  Outlier(0.05);
 };
 R_Date("C4c4-AA-69183", 37580, 780)
 {
  Outlier(0.05);
 };
 R_Date("C4c4-AA-69180", 37300, 1800)
 {
  Outlier(0.05);
 };
 R_Date("C4c4-AA-69179", 37000, 1600)
 {
  Outlier(0.05);
 };
 R_Date("C4c4-AA-69185", 36990, 720)
 {
  Outlier(0.05);
 };
 R_Date("C4c4-AA-69181", 36800, 860)
 {
  Outlier(0.05);
 };
};
Boundary("Transition Proto+Auri C 4c4/C 4b2");
Phase("C 4b2")
{
 R_Date("C4b2-OxA-X-2698-50", 35150, 650)
 {
  Outlier(0.05);
 };
 R_Date("C4b2-OxA-34636", 35050, 650)
```

```
  {
   Outlier(0.05);
  };
  R_Date("C4b2-OxA-34773", 34950, 600)
  {
   Outlier(0.05);
  };
  R_Date("C4b2-OxA-34637", 34850, 600)
  {
   Outlier(0.05);
  };
 };
 Boundary("Transition Proto+Auri C 4b2/Early Aurignacian C 4b1");
 Phase("C 4b1")
 {
  R_Date("C4b1-OxA-34635", 35250, 650)
  {
   Outlier(0.05);
  };
  R_Date("C4b1-OxA-34633", 35250, 650)
  {
   Outlier(0.05);
  };
  R_Date("C4b1-OxA-34772", 34950, 600)
  {
   Outlier(0.05);
  };
  R_Date("C4b1-OxA-34634", 34700, 600)
  {
   Outlier(0.05);
  };
 };
 Boundary("End Early Aurignacian C 4b1");
};
Sequence()
{
 Boundary("=Start Protoaurignacian C 4d1");
 Date("Only Protoaurignacian");
 Boundary("=Transition Protoaurignacian C 4d1/Proto+Auri C 4c4");
};
Sequence()
{
 Boundary("=Transition Protoaurignacian C 4d1/Proto+Auri C 4c4");
 Date("Proto+Auri");
 Boundary("=Transition Proto+Auri C 4b2/Early Aurignacian C 4b1");
};
Sequence()
{
 Boundary("=Transition Proto+Auri C 4b2/Early Aurignacian C 4b1");
 Date("Early Aurignacian");
 Boundary("=End Early Aurignacian C 4b1");
```

```
 };
};
```

Gatzarria

Gatzarria is close to Isturitz in the south-eastern part of the Aquitaine region, in the Basque region of France. This site has yielded a sequence of Aurignacian industries (Protoaurignacian, Classic Aurignacian, and Late Aurignacian), a Châtelperronian layer, and at the bottom different Mousterian layers (including the Vasconian Mousterian). In the paper of Barshay-Szmidt et al. (2012) they dated two samples from Vasconian Mousterian that gave infinite ages, two samples from Protoaurignacian from layer Cjn2 and two from the top layer of classic Aurignacian level Cbf. We built a new Bayesian model following Barshay-Szmidt et al. (2012) only for the two phases knowing that there is the Mousterian that is out of the radiocarbon age at the bottom followed by the Châtelperronian without dates. The Bayesian model does not provide a realistic output for the Vasconian Mousterian since the two radiocarbon dates are actually out of the range of radiocarbon and show that this deposit is older than 47,400 and 50,300 ^{14}C BP.

Bayesian Modelled Boundaries and Duration of the phases provided by the IntCal13 (Reimer et al., 2013) using OxCal 4.3 (Ramsey, 2009) are the following:

Gatzarria	**Modelled (BP)**			
Indices Amodel 39.7 Aoverall 50.3	**from**	**to**	**from**	**to**
	68,20%		**95,40%**	
End Cbf Classic Aurignacian	39220	38200	39870	37310
Classic Aurignacian	39320	38430	39870	37800
Transition CJK1/Cbci-Cbf Classic Aurignacian	39430	38630	39900	38210
Transition CJK2/CJK1	39770	38880	40370	38500
Protoaurignacian	40130	39010	41050	38600
Start CJK2 ProtoAurignacian	40510	38930	41940	38640

In red are the ranges taken for building the bars in the graph in Figure 3 in the main text

CQL Code:

```
Plot()
 {
  Outlier_Model("General",T(5),U(0,4),"t");
  Sequence()
  {
   Boundary("Start Cjn2 ProtoAurignacian");
   Phase("ProtoAurignacian")
   {
    R_Date("Gtz-Cjn2-OxA- 22553", 33800, 550)
    {
     Outlier(0.05);
    };
    R_Date("Gtz-Cjn2-OxA- 22554", 36300, 700)
    {
```

```
   Outlier(0.05);
  };
 };
 Boundary("Transition Cjn2/Cjn1");
 Boundary("Transition Cjn1/Cbci-Cbf Classic Aurignacian");
 Phase("Classic Aurignacian")
 {
  R_Date("Gtz-Cbf-OxA- 22556", 34250, 550)
  {
   Outlier(0.05);
  };
  R_Date("Gtz-Cbf-OxA- 22555", 34400, 550)
  {
   Outlier(0.05);
  };
 };
 Boundary("End Cbf Classic Aurignacian");
};
Sequence()
{
 Boundary("=Start Cjn2 ProtoAurignacian");
 Date("Protoaurignacian");
 Boundary("=Transition Cjn2/Cjn1");
};
Sequence()
{
 Boundary("=Transition Cjn1/Cbci-Cbf Classic Aurignacian");
 Date("Classic Aurignacian");
 Boundary("=End Cbf Classic Aurignacian");
};
};
```

Langued-Roussillon region

Régismont-le-Haut

This site is one of the few Aurignacian open-air sites in southern France. The site is located in the department of Hérault, in the Langued-Roussillon region. It has yielded archaeological evidence of Upper Palaeolithic with Aurignacian levels. In Szmidt et al. 2018b they show five new dated samples, three come from sector S56 in Locus 1 dated by NSF-Arizona and at IsoTrace. Two samples were combined since they come from the same fireplace. Two charcoal samples from sector S72 in Locus 2 were dated at ORAU. Even if there is a divergence of dates between the two loci, we produced two different Bayesian models for the two different loci and inserted in Figure 3 in the main text, as was done in Barshay-Szmidt et al. (2018b) to determine which are most comparable with other Aurignacian sites.

Bayesian Modelled Boundaries and Duration of the phases in the two Loci provided by the IntCal13 (Reimer et al., 2013) using OxCal 4.3 (Ramsey, 2009) are the following:

Régismont-le-Haut Locus 1	**Modelled (BP)**			
Indices Amodel 103.8 Aoverall 104	**from**	**to**	**from**	**to**
	68,20%		**95,40%**	
End Aurignacian in Locus 1	32780	30490	33020	26100
Aurignacian in Locus 1	33340	31400	36040	28830
Start Locus 1	34240	31890	39170	31640
Régismont-le-Haut Locus2	**Modelled (BP)**			
Indices Amodel 98.9 Aoverall 99.8	**from**	**to**	**from**	**to**
	68,20%		**95,40%**	
End Loci 2	36490	34430	36590	30660
Aurignacian in Loci 2	37580	35420	40350	32910
Start Aurignacian in Loci 2	38630	36260	43190	36200

In red are the ranges taken for building the bars in the graph in Figure 3 in the main text

CQL Code:

```
Plot()
 {
  Outlier_Model("General",T(5),U(0,4),"t");
  Sequence("Regismont-le-Haut Locus 1")
  {
   Boundary("Start Aurignacian Loci 1");
   Phase("Loci 1")
   {
    R_Date("TO-1178", 28550, 340)
    {
     Outlier(0.05);
    };
    R_Date("AA69175 and AA69176", 28170, 430)
    {
     Outlier(0.05);
    };
   };
   Boundary("End Aurignacian in Loci 1");
  };
  Sequence()
  {
   Boundary("=Start Aurignacian Loci 1");
   Date("Aurignacian in Loci 1");
   Boundary("=End Aurignacian in Loci 1");
  };
```

```
 };
Plot()
 {
  Outlier_Model("General",T(5),U(0,4),"t");
  Sequence("Regismont-le-Haut Locus 2")
  {
   Boundary("Start Aurignacian in Loci 2");
   Phase("Loci 2")
   {
    R_Date("OxA-20982", 32220, 200)
    {
     Outlier(0.05);
    };
    R_Date("OxA-22835", 32900, 270)
    {
     Outlier(0.05);
    };
   };
   Boundary("End Aurignacian Loci 2");
  };
  Sequence()
  {
   Boundary("=Start Aurignacian in Loci 2");
   Date("Aurignacian in Loci 2");
   Boundary("=End Aurignacian Loci 2");
  };
 };
```

La Crouzade

The site is located in the Langued-Roussillon region not far from Régismont-le-Haut. The site has yielded archaeological evidence for several Mousterian layers (C8 to C6) followed at the top by the Aurignacian. Following the main stratigraphic division and the radiocarbon dates and ESR-UTh ages in Saos et al. (2019), we built a new Bayesian model. The duration of the Mousterian layers C7 and C6 could be an artificial range due to the wide error range of the ESR-UTh dates. Even if they considered the direct date of the *Homo sapiens* too young and probably due to contamination, we insert the ^{14}C date in the Bayesian model in the Aurignacian layer C5, but the result needs to be taken as suggestive, and probably additional dates will be processed in the near future.

Bayesian Modelled Boundaries and Duration of the phases provided by the IntCal13 (Reimer et al., 2013) using OxCal 4.3 (Ramsey, 2009) are the following:

la Crouzade	Modelled (BP)			
Indices Amodel 81.5 Aoverall 77.9	**from**	**to**	**from**	**to**
	68,20%		**95,40%**	
End Aurignacian C5	35680	33930	36080	30680
Aurignacian C5	36630	34650	39220	32690
Transition Mousterian C6/Aurignacian C5	37690	35580	40460	35320
Transition Mousterian C6/Aurignacian C5	37690	35580	40460	35320
Mousterian C7-C6	42210	37880	43610	36270
Transition Mousterian C8/C7	44320	41690	45280	40250
Transition Mousterian C8/C7	44320	41690	45280	40250
Mousterian C8-C6	46060	43330	48040	41500
Start Mousterian C8	47560	44740	49970	...

In red are the ranges taken for building the bars in the graph in Figure 3 in the main text

CQL Code:

```
Plot()
 {
  Outlier_Model("General",T(5),U(0,4),"t");
  Sequence()
  {
   Boundary("Start Mousterian C8");
   Phase("C8")
   {
    R_Date("PoZ-37967", 43400, 1400)
    {
     Outlier(0.05);
    };
    R_Date("PoZ-37966", 42200, 1000)
    {
     Outlier(0.05);
    };
    R_Date("PoZ-66106", 38700, 900)
    {
     Outlier(0.05);
    };
   };
   Boundary("Transition Mousterian C8/C7");
   Phase("C7")
   {
    Age("Cz1402", N(41000,2000))
    {
     Outlier(0.05);
```

```
   };
  };
  Boundary("Transition Mousterian C7/C6");
  Phase("C6")
  {
   Age("Cz1401", N(42000,3000))
   {
    Outlier(0.05);
   };
  };
  Boundary("Transition Mousterian C6/Aurignacian C5");
  Phase("C5")
  {
   R_Combine("La Crouzade VI")
   {
    Outlier(0.05);
    R_Date("OxA-X-2635-38", 31200, 400);
    R_Date("ERL-9415", 30640, 640);
   };
   R_Date("OxA-37723", 32060, 250)
   {
    Outlier(0.05);
   };
  };
  Boundary("End Aurignacian C5");
 };
 Sequence()
 {
  Boundary("=Start Mousterian C8");
  Date("Mousterian C8-C6");
  Boundary("=Transition Mousterian C8/C7");
 };
 Sequence()
 {
  Boundary("=Transition Mousterian C8/C7");
  Date("Mousterian C7-C6");
  Boundary("=Transition Mousterian C6/Aurignacian C5");
 };
 Sequence()
 {
  Boundary("=Transition Mousterian C6/Aurignacian C5");
  Date("Aurignacian C5");
  Boundary("=End Aurignacian C5");
 };
};
```

References:

AUBRY, T., DIMUCCIO, L. A., BUYLAERT, J.-P., LIARD, M., MURRAY, A. S., THOMSEN, K. J. & WALTER, B. 2014. Middle-to-Upper Palaeolithic site formation processes at the Bordes-Fitte rockshelter (Central France). *Journal of Archaeological Science,* 52**,** 436-457.

BARSHAY-SZMIDT, C., ANDERSON, L., LEJAY, M., THÉRY-PARISOT, I., BURR, G. S., MENSAN, R. & BON, F. 2018b. Out of the Cave and into the Light: Perspectives and Challenges of Radiocarbon Dating an Open-Air Aurignacian Site (Régismont-le-Haut, Mediterranean France). *Journal of Paleolithic Archaeology,* 1**,** 247-279.

BARSHAY-SZMIDT, C., NORMAND, C., FLAS, D. & SOULIER, M.-C. 2018a. Radiocarbon dating the Aurignacian sequence at Isturitz (France): Implications for the timing and development of the Protoaurignacian and Early Aurignacian in western Europe. *Journal of Archaeological Science: Reports,* 17**,** 809-838.

BARSHAY-SZMIDT, C. C., EIZENBERG, L. & DESCHAMPS, M. 2012. Radiocarbon (AMS) dating the Classic Aurignacian, Proto-Aurignacian and Vasconian Mousterian at Gatzarraia Cave (Pyrenees-Atlantiques, France). *PALEO,* 23**,** 11-38.

BOURRILLON, R., WHITE, R., TARTAR, E., CHIOTTI, L., MENSAN, R., CLARK, A., CASTEL, J. C., CRETIN, C., HIGHAM, T., MORALA, A., RANLETT, S., SISK, M., DEVIÈSE, T. & COMESKEY, D. J. 2018. A new Aurignacian engraving from Abri Blanchard, France: Implications for understanding Aurignacian graphic expression in Western and Central Europe. *Quaternary International,* 491**,** 46-64.

FLOSS, H., HOYER, C. & WÜRSCHEM, H. 2016. Le Châtelperronien de Germolles (Grotte de La Verpillière I, commune de Mellecey, Saône-et-Loire, France). *PALEO. Revue d'archéologie préhistorique***,** 149-176.

FLOSS, H., HOYER, C. T., HECKEL, C. & TARTAR, É. 2015. The Aurignacian in Southern Burgundy. In: WHITE R. & BOURRILLON R., with the collaboration of Bon. F. (eds.) Palethnologie. Archéologie et sciences humaines. Aurignacian Genius: Art, Technology and Society of the First Modern Humans in Europe, . New York University, P@lethnology: Proceedings of the International Symposium, April 08-10 2013.

FROUIN, M., LAHAYE, C., VALLADAS, H., HIGHAM, T., DEBÉNATH, A., DELAGNES, A. & MERCIER, N. 2017. Dating the Middle Paleolithic deposits of La Quina Amont (Charente, France) using luminescence methods. *Journal of Human Evolution,* 109**,** 30-45.

GRAVINA, B., BACHELLERIE, F., CAUX, S., DISCAMPS, E., FAIVRE, J.-P., GALLAND, A., MICHEL, A., TEYSSANDIER, N. & BORDES, J.-G. 2018. No Reliable Evidence for a Neanderthal-Châtelperronian Association at La Roche-à-Pierrot, Saint-Césaire. *Scientific Reports,* 8**,** 15134.

GRAVINA, B. & DISCAMPS, E. 2015. MTA-B or not to be? Recycled bifaces and shifting hunting strategies at Le Moustier and their implication for the late Middle Palaeolithic in southwestern France. *Journal of Human Evolution,* 84**,** 83-98.

GUÉRIN, G., FROUIN, M., TALAMO, S., ALDEIAS, V., BRUXELLES, L., CHIOTTI, L., DIBBLE, H. L., GOLDBERG, P., HUBLIN, J.-J., JAIN, M., LAHAYE, C., MADELAINE, S., MAUREILLE, B., MCPHERRON, S. J. P., MERCIER, N., MURRAY, A. S., SANDGATHE, D., STEELE, T. E., THOMSEN, K. J. & TURQ, A. 2015. A multi-method luminescence dating of the Palaeolithic sequence of La Ferrassie based on new excavations adjacent to the La Ferrassie 1 and 2 skeletons. *Journal of Archaeological Science,* 58**,** 147-166.

HIGHAM, T., DOUKA, K., WOOD, R., RAMSEY, C. B., BROCK, F., BASELL, L., CAMPS, M., ARRIZABALAGA, A., BAENA, J., BARROSO-RUIZ, C., BERGMAN, C., BOITARD, C., BOSCATO, P., CAPARROS, M., CONARD, N. J., DRAILY, C., FROMENT, A., GALVAN, B., GAMBASSINI, P., GARCIA-MORENO, A., GRIMALDI, S., HAESAERTS, P., HOLT, B., IRIARTE-CHIAPUSSO, M.-J., JELINEK, A., JORDA PARDO, J. F., MAILLO-FERNANDEZ, J.-M., MAROM, A., MAROTO, J., MENENDEZ,

M., METZ, L., MORIN, E., MORONI, A., NEGRINO, F., PANAGOPOULOU, E., PERESANI, M., PIRSON, S., DE LA RASILLA, M., RIEL-SALVATORE, J., RONCHITELLI, A., SANTAMARIA, D., SEMAL, P., SLIMAK, L., SOLER, J., SOLER, N., VILLALUENGA, A., PINHASI, R. & JACOBI, R. 2014. The timing and spatiotemporal patterning of Neanderthal disappearance. *Nature,* 512**,** 306-309.
HIGHAM, T., JACOBI, R., BASELL, L., RAMSEY, C. B., CHIOTTI, L. & NESPOULET, R. 2011. Precision dating of the Palaeolithic: A new radiocarbon chronology for the Abri Pataud (France), a key Aurignacian sequence. *Journal of Human Evolution,* 61**,** 549-563.
HUBLIN, J.-J., SPOOR, F., BRAUN, M., ZONNEVELD, F. & CONDEMI, S. 1996. A late Neanderthal associated with Upper Palaeolithic artefacts. *Nature,* 381**,** 224-226.
HUBLIN, J.-J., TALAMO, S., JULIEN, M., DAVID, F., CONNET, N., BODU, P., VANDERMEERSCH, B. & RICHARDS, M. P. 2012. Radiocarbon dates from the Grotte du Renne and Saint-Césaire support a Neandertal origin for the Châtelperronian. *PNAS,* 109**,** 18743-18748.
MCPHERRON, S. P., TALAMO, S., GOLDBERG, P., NIVEN, L., SANDGATHE, D., RICHARDS, M. P., RICHTER, D., TURQ, A. & DIBBLE, H. L. 2012. Radiocarbon dates for the late Middle Palaeolithic at Pech de l'Azé IV, France. *Journal of Archaeological Science,* 39**,** 3436-3442.
RAMSEY, C. B. 2009. Dealing with outliers and offsets in radiocarbon dating. *Radiocarbon,* 51**,** 1023-1045.
REIMER, P. J., BARD, E., BAYLISS, A., BECK, J. W., BLACKWELL, P. G., BRONK RAMSEY, C., GROOTES, P. M., GUILDERSON, T. P., HAFLIDASON, H., HAJDAS, I., HATTÉ, C., HEATON, T. J., HOFFMANN, D. L., HOGG, A. G., HUGHEN, K. A., KAISER, K. F., KROMER, B., MANNING, S. W., NIU, M., REIMER, R. W., RICHARDS, D. A., SCOTT, E. M., SOUTHON, J. R., STAFF, R. A., TURNEY, C. S. M. & VAN DER PLICHT, J. 2013. IntCal13 and Marine13 Radiocarbon Age Calibration Curves 0–50,000 Years cal BP. *Radiocarbon,* 55**,** 1869-1887.
SAOS, T., GRÉGOIRE, S., BAHAIN, J.-J., HIGHAM, T., MOIGNE, A.-M., TESTU, A., BOULBES, N., BACHELLERIE, M., CHEVALIER, T., BECAM, G., DURAN, J.-P., ALLADIO, A., ORTEGA, M. I., DEVIÈSE, T. & XIAO, Q. 2019. The Middle and Upper Palaeolithic at La Crouzade cave (Gruissan, Aude, France): New excavations and a chronostratigraphic framework. *Quaternary International*.
SZMIDT, C. C., BROU, L. & JACCOTTEY, L. 2010b. Direct radiocarbon (AMS) dating of split-based points from the (Proto)Aurignacian of Trou de la Mère Clochette, Northeastern France. Implications for the characterization of the Aurignacian and the timing of technical innovations in Europe. *Journal of Archaeological Science,* 37**,** 3320-3337.
SZMIDT, C. C., MONCEL, M.-H. & DAUJEARD, C. 2010a. New data on the Late Mousterian in Mediterranean France: First radiocarbon (AMS) dates at Saint-Marcel Cave (Ardèche). *Palevol,* 9**,** 185-199.
TALAMO, S., SORESSI, M., ROUSSEL, M., RICHARDS, M. & HUBLIN, J.-J. 2012. A radiocarbon chronology for the complete Middle to Upper Palaeolithic transitional sequence of Les Cottés (France). *Journal of Archaeological Science,* 39**,** 175-183.
THOMSEN, K. J., MURRAY, A. S., BUYLAERT, J. P., JAIN, M., HANSEN, J. H. & AUBRY, T. 2016. Testing single-grain quartz OSL methods using sediment samples with independent age control from the Bordes-Fitte rockshelter (Roches d'Abilly site, Central France). *Quaternary Geochronology,* 31**,** 77-96.
VERNA, C., DUJARDIN, V. & TRINKAUS, E. 2012. The Early Aurignacian human remains from La Quina-Aval (France) Original Research Article. *Journal of Human Evolution,* 62**,** 605-617.
WELKER, F., HAJDINJAK, M., TALAMO, S., JAOUEN, K., DANNEMANN, M., DAVID, F., JULIEN, M., MEYER, M., KELSO, J., BARNES, I., BRACE, S., KAMMINGA, P.,

FISCHER, R., KESSLER, B. M., STEWART, J. R., PÄÄBO, S., COLLINS, M. J. & HUBLIN, J.-J. 2016. Palaeoproteomic evidence identifies archaic hominins associated with the Châtelperronian at the Grotte du Renne. *Proceedings of the National Academy of Sciences,* 113**,** 11162-11167.

WHITE, R., BOURRILLON, R., MENSAN, R., CLARK, A., CHIOTTI, L., HIGHAM, T., RANLETT, S., TARTAR, E., MORALA, A. & SOULIER, M.-C. 2018. Newly discovered Aurignacian engraved blocks from Abri Cellier: History, context and dating. Quaternary International, 498, 99-125.

WHITE, R., MENSAN, R., BOURRILLON, R., CRETIN, C., HIGHAM, T. F. G., CLARK, A. E., SISK, M. L., TARTAR, E., GARDÈRE, P., GOLDBERG, P., PELEGRIN, J., VALLADAS, H., TISNÉRAT-LABORDE, N., DE SANOIT, J., CHAMBELLAN, D. & CHIOTTI, L. 2012. Context and dating of Aurignacian vulvar representations from Abri Castanet, France. *Proceedings of the National Academy of Sciences,* 109**,** 8450-8455.